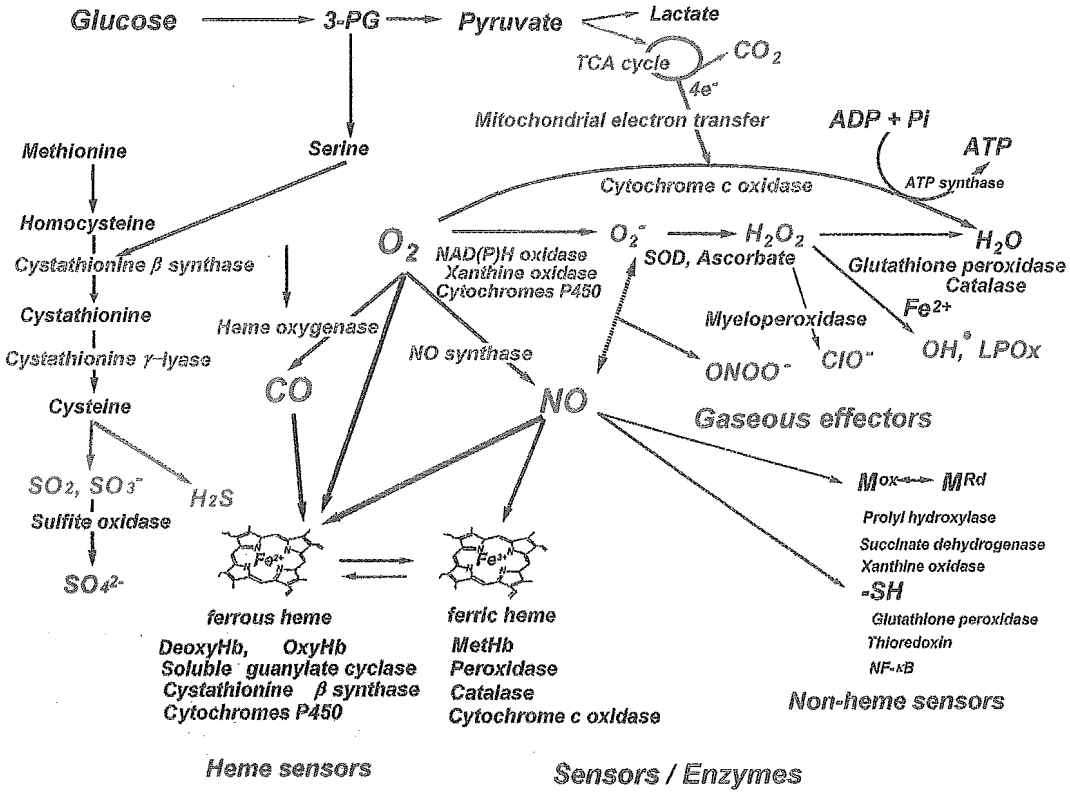

FIG. 1. Metabolic links between cellular energetics and synthesis of gaseous mediators in mammals. Cited from reference 32 with permission.

DETECTING ROS FROM NEUTROPHILS *IN VITRO* AND *IN VIVO*

Neutrophils are one of the major sources that generate large amounts of ROS under stimulated conditions (38). In 1987, we attempted for the first time a real-time visualization of ROS to specify when and where the cells are activated during the process of their tissue recruitment. To this end, we applied an ultrasensitive photon-counting imaging system combined with intravital microscopy: this system enabled us to acquire two-dimensional information on the chemiluminescence emission through oxyradical burst of neutrophils in real time. When neutrophils in culture were stimulated with opsonized zymosan in the presence of luminol, a chemiluminescence probe, they exhibited site-specific photonic burst colocalized with the restricted regions of phagosomes (28). On the other hand, when stimulated with phorbol myristate acetate, which activates NADPH oxidase, the luminol-dependent chemiluminescence was little, if any. The addition of the calcium ionophore A23187, however, induced massive and diffuse elevation of the chemiluminescence (29). As these photonic activities were abolished by catalase or azide or by replacement with the chloride-free medium, a major ROS responsible for this event appeared to derive from the H_2O_2-myeloperoxidase-Cl^- system, such as hypochlorous anion (ClO^-), under the given experimental conditions.

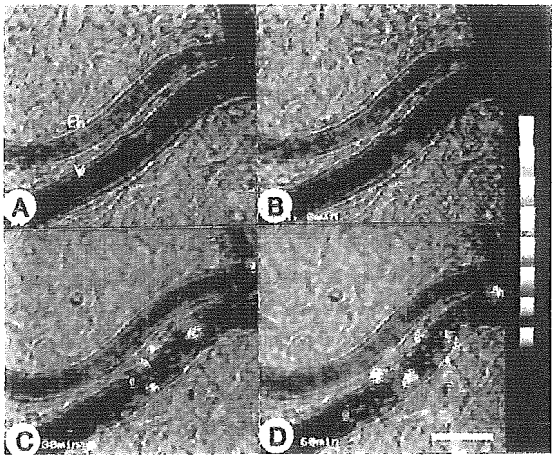

FIG. 2. *In vivo* visualization of oxyradical burst during leukocyte–endothelial cell interactions in postcapillary venules of endotoxemic rats. (**A** and **B**) Representative micrographs showing basal chemiluminescence activities detected in the absence or presence of the superfusion of luminol, a chemiluminescence probe, on the mesenteric microvessels. (**C** and **D**) Micrographs showing effects of intravenous administration of lipopolysaccharide O-111B4 at 2 mg/kg/h, indicating an increase in photonic burst from adherent leukocytes in the venule (v), but not in the arteriole (a). Bar = 50 μm. Cited from reference 28 with permission.

We then applied this system to visualize ROS generated from activated neutrophils *in vivo* (24, 27, 30). Figure 2 illustrates representative micrographs showing spatial and temporal alterations in luminol-dependent chemiluminescence in the mesenteric microvessels of endotoxemic rats (24). As seen, the photonic activities were elevated in parallel with an increase in the number of adherent neutrophils. Most importantly, the activities coincided with venular endothelial walls with adherent cells, whereas those were absent in arteriolar walls or the interstitial space. This suggests that the interface between venular endothelium and adherent leukocytes serves as a primary domain for the oxidant formation during their tissue recruitment. Pretreatment of superoxide dismutase (SOD) in circulation caused elimination of neutrophil adhesion leading to the abolition of the chemiluminescence. This result was consistent with the fact that SOD increases the velocity of venular leukocyte rolling and thereby diminishes their stationary adhesion in response to proinflammatory stimuli or ischemia–reperfusion (35). Other proinflammatory stimuli, such as platelet-activating factor and interleukin-8, also elicited comparable oxidative burst from adherent neutrophils (30, 34), and the SOD administration again attenuated the photonic responses in parallel with a reduction of the adherent cells. Upon exposure to these stimuli, neutrophils adherent to endothelium appeared to exhibit secretagogue activation (*e.g.*, azurophilic degranulation) and utilize ROS to inactivate endogenous proteinase inhibitors and to activate collagenase to enhance proteolytic activities required for cell migration (38). However, such an activation of ROS generation is unlikely a prerequisite for neutrophil migration, because leukotriene B_4-induced leukocyte adhesion and migration did not coincide with any detectable amounts of the chemiluminescence (27). This observation is also consistent with the failure of SOD to attenuate the leukotriene B_4-elicited adhesion response. Mechanisms by which superoxide mediates leukocyte rolling and adhesion have been considered to involve activation of P-selectin expression on venular endothelial cells (16, 22, 31). As NO cancels superoxide, a tenuous balance between these species serves as a determinant of tissue recruitment of neutrophils in postcapillary venules. Thus, establishment of the method to collect spatial and temporal information on NO in microvascular systems became necessary.

MICROVASCULAR DELIVERY OF NO AND REGULATION OF MICROVASCULAR FUNCTION

As NO was first recognized as a critical modulator of venular leukocyte adhesion in 1991 (16), its interactions with ROS and their functional outcomes on adhesion responses of leukocytes in microcirculation have been discussed extensively in varied disease models. Bioavailability of NO in microcirculation depends on expression of NO synthases (NOSs), which are divided into three isoforms; neuronal (nNOS or NOS1), inducible NOS (iNOS or NOS2), and endothelial NOS (eNOS or NOS3) (19). NO released from the constitutive isozymes has been shown to play important roles for functional integrity of vascular systems under normal conditions. Such roles include maintenance of vascular patency to guarantee ample blood supply, prevention of unnecessary adhesion of platelets and leukocytes (19), stabilization of mast cells (17), regulation of vascular permeability, and modulation of vascular remodeling involving proliferation of vascular smooth muscle cells. When endogenous NO was suppressed by the enzyme inhibitors, apparent ROS generation in microvascular endothelium or in mast cells was markedly elevated and resulted in adhesion of leukocytes through mechanisms involving endothelial P-selectin expression (31).

Until now, most NO available for vascular walls has been thought to derive mainly from endothelial cells, which express NOS3. However, our studies have revealed that the local availability of NO in arterioles and that in venules appears, to depend on distinct enzymes, such as NOS1 and NOS3, respectively, suggesting distinct mechanisms for delivery of NO among different hierarchy of microvessels (12). This concept has been achieved by real-time assessment of microvascular NO generation using 4,5-diaminofluorescein diacetate (DAF-2DA) microfluorography. DAF-2DA is a membrane-permeable fluorescence precursor sensing intracellular NO generation (15). As seen in Fig. 3, the fluorescence occurred comparably in arteriolar and venular walls, and also in mast cells in the interstitium. The immunohistochemistry for NOS1 and NOS3 in the rat mesentery showed that the proximal arterioles express both isozymes, whereas the distal ones with smaller diameters express only NOS1, but little NOS3, if any. This was the case not only in the mesentery, but also in brain. Until now, other studies have suggested that conducting arteries proximal to microvessels mainly use NO derived from its own endothelium expressing NOS3 to maintain their patency to supply blood flow, whereas smaller arterioles could mainly use NO-independent mechanisms (*e.g.*, endothelium-derived hyperpolarizing factor) for vasorelaxation (37). Most of the previous experiments suggesting lesser roles of NO in modulation of arteriolar tone were collected from the *ex vivo* perfused vessels undergoing the denervated and connective tissue-free preparation, and could thus overlook roles of NOS1 around arterioles. Such an underestimation of the paracrine source of NO in arterioles has been revised by our studies.

On the other hand, endothelia of capillaries and venules seem to express NOS3. This notion was supported by the observation that 7-nitroindazole (7-NI) induced only modest activation of venular leukocyte adhesion as compared with the same concentration of N^{ω}-nitro-L-arginine methyl ester (L-NAME). As mentioned in the previous section, a tenuous balance between NO and superoxide anion could determine susceptibility of mast cells to degranulation stimuli, and NO serves as a stabilizer of the exocytosis *in vitro* and *in vivo* (17). In both arterioles and venules, sufficient concentrations of NOS inhibitors significantly attenuated the NO-associated fluorescent signals, but only partly; ~40% of the signals remained as the basal activities. Such a low susceptibility to NOS inhibitors raised an important possibility of another source of NO derived from nonenzymatic origins besides locally expressed NOS isozymes (Fig 3). *S*-Nitrosyl hemoglo-

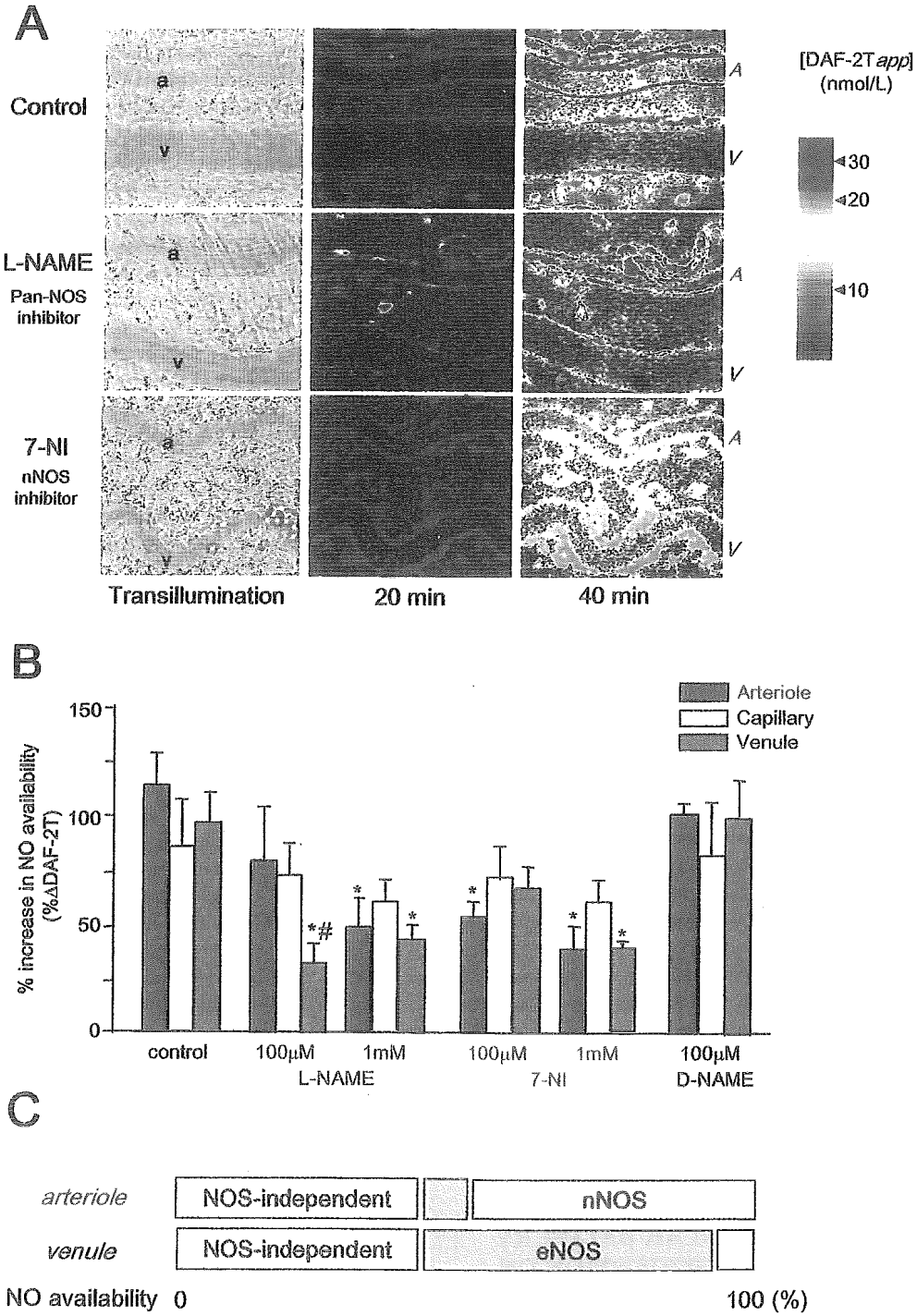

FIG. 3. Representative pictures showing microvascular NO distribution revealed by digital microfluorography using NO^+-sensitive diaminofluorescein (DAF). (A) Pseudocolor representation of DAF fluorescence in the rat mesenteric microcirculation and sensitivity to locally applied NOS inhibitors such as L-NAME and 7-NI, a potent NOS1 inhibitor. *A* and *V* denote a pair of arteriole and venule. (B) Semiquantitative analyses of the sensitivity of DAF fluorescence to the NOS inhibitors. Greater susceptibility of arteriolar signals to 7-NI than to L-NAME suggest that NOS1 supports NO availability in arterioles. Note the presence of NOS-independent fraction of the fluorescence even in the presence of sufficient amounts of the inhibitors. (C) A schematic diagram of difference in sources of NO between arterioles and venules. A and B are cited from reference 12 with permission.

bin in circulating erythrocytes that could release NO upon a reduction of local oxygen pressure is among such sources taken into account. Considering the recent observation that a drop in the intravascular oxygen tension occurs first in the distal arterioles rather than in capillaries (10), it can be hypothesized that such an alternative source explains the presence of the L-NAME- and 7-NI-insensitive fraction of local NO availability. However, as erythrocytes are thought to consititute a metabolic sink for NO and the gas can readily bind to the hemoglobin-heme in the cells to serve as an allosteric regulator of oxygen transport, roles of *S*-nitrosyl compounds as an NO reservoir should be further examined carefully (40).

MECHANISTIC BIOPROBING OF SOLUBLE GUANYLATE CYCLASE REVEALS INTERACTIONS BETWEEN NO AND CO *IN VIVO*

CO has been considered a gaseous mediator analogous to NO that contributes to signal transduction in neurovascular systems. This gas is one of the reaction products of heme oxygenase (HO), the enzyme that catalyzes protoheme IX into biliverdin-IXα and ferrous iron. Biliverdin-IXα is converted to bilirubin-IXα through the reaction of biliverdin reductase and serves as a potent antioxidant that ameliorates inflammatory responses (8, 36). As described later, in the liver, CO serves as a vasorelaxant for sinusoids that activates soluble guanylate cyclase (sGC) in hepatic stellate cells, liver-specific pericytes; this mechanism explains why this organ can maintain low vascular resistance to ensure ample blood supply from portal venous system (26, 32, 33).

In mammals, HO exists in two forms: HO-1 and HO-2 (36). HO-1 is induced by stressors such as cytokines, heavy metals, hypoxia and ROS. Excess NO could also cause the HO-1 induction (26). By contrast, HO-2 appears to be constitutive. The HO/CO system may regulate function of heme proteins and enzymes in several ways: in the liver, cytochrome P450 (but not other heme enzymes such as catalase) contains ferrous heme under normoxic conditions and thus is susceptible to inhibition by CO (18). By contrast, cytochrome oxidase in mitochondria is unlikely to be affected by CO, because its prosthetic heme is predominantly in the ferric state; thus, the susceptibility of each heme protein to this gas greatly depends on its redox states (26). HO catalyzes prosthetic heme of cytochromes P450 and could reduce the holoenzymes. The HO reaction requires reducing equivalents supplied by NADPH, and thus its competition for the electron pool could interfere with other enzyme reactions. CO shares several heme proteins as signal transducers with NO and could fine-tune functions of the receptors through distinct mechanisms. One such example is the effect of these gases on hemoglobin allostery: as widely known, CO stabilizes the six-coordinated form of the prosthetic heme and increases the affinity of molecular oxygen in other subunits, whereas NO binds to the α subunit of the heme and breaks the proximal histidine-Fe bond, forming a five-coordinated nitrosyl heme complex to decrease the affinity of oxygen in β subunits.

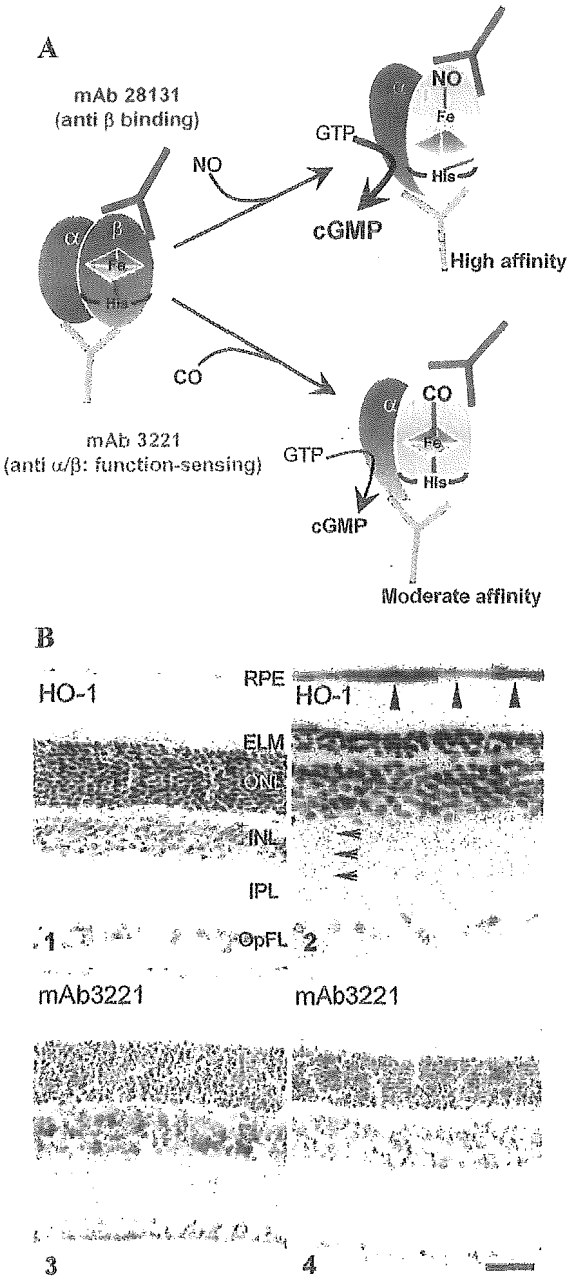

FIG. 4. Mechanistic bioprobing of gas-dependent regulation of sGC by mAb3221 and mAb28131. (**A**) Functional epitopes responsible for detecting the activation of the enzyme by NO and CO. (**B**) Application of the antibody 3221 to immunohistochemistry of rat retina exposed to sustained light exposure. The light exposure causes stress responses of HO-1 throughout the entire retinal cell layers (panel 2). Distinct patterns of sGC activation among the layers are evident (panel 4). The HO-1 induction caused an inhibition of the sGC activities in the inner plexiform layer (IPL) where ample NO is available. By contrast, it causes activation in the external limiting membrane (ELM) where NO is limited. INL, inner nuclear layer; ONL, outer nuclear layer; OpFL, optic nerve fiber layer; RPE, retinal pigment epithelium. Bar = 30 μm. Panel B was cited from reference 11 with permission.

Identical structural differences in the prosthetic heme also explain the distinct ability of NO versus CO to activate sGC, a common signal transducer for both gases (14, 26).

In biological systems, multiple gases might share the individual signal transducer for fine-tuning cell functions, but little evidence for demonstrating this hypothesis has been available. In other words, development of molecular probes that can sense the ligand binding and/or specific conformational changes allowed us to examine the behavior of gaseous mediators *in vivo*. Newly generated monoclonal antibodies (mAbs) against sGC, mAb28131 and mAb3221, have made it possible to examine the activation state of the enzyme regulated by NO and CO in the rat retina, where two gases and one transducer might play a role in cyclic GMP-dependent regulation of the tissue function. mAb3221 recognizes a regiospecific structure determined by the two subunits of a native sGC protein. Characterization of mAbs by surface plasmon resonance technology revealed that mAb3221 increases its affinity to the antigen by 100- or 10-fold in the presence of NO or CO, respectively. These results suggest that mAb3221 recognizes a regiospecific epitope formed by α and β subunits of the enzyme that could be altered by binding of gas mediators to the heme (Fig. 4A). On the other hand, the affinity of mAb28131 to the enzyme remained constant regardless (11). The results conform to our idea that comparison of immunoreactivities between the two distinct mAbs enables us to assess local sGC regulation by NO and CO *in vivo* using immunohistochemical approaches.

In these studies, we used rat retina as an experimental system because its well defined anatomical layers consisting of specific cell types enabled us to examine spatial relationships between NO- and CO-generating enzymes and their receptor protein, sGC. In this tissue, sGC was localized mainly in Mueller's glia cells, which constitute the tissue-supporting interface between microcirculation and the neural system, and partly in on-type bipolar cells, the second neuron for phototransduction. Direct detection of the sGC function with mAb3221 led us to propose a novel hypothesis to explain the long-standing controversy concerning synergistic or antagonistic interactions of the two diatomic gases to regulate sGC activities *in vivo*: The effect of CO on modulating sGC activity is not static, but dynamic in that low tissue NO makes CO a stimulatory modulator of sGC, whereas high tissue NO makes CO an inhibitory one. Administration of L-arginine enhanced, and that of the NOS inhibitor attenuated, mAb3221 immunoreactivities. Blockade of HO by the competitive inhibitor zinc protoporphyrin-IX elicited marked enhancement of the immunoreactivities, suggesting that endogenous CO plays a modulatory role in NO-mediated sGC activation.

It should be noted that sustained exposure to visible light caused HO-1 induction throughout the entire retina, but resulted in heterogenous responses of sGC activation among different layers. HO-1-derived CO suppressed sGC in inner plexiform and nuclear layers, while activating it in external limiting membrane (Fig. 4B). This event appeared to result from heterogenous availability of NO among the layers. NO could be ample in inner plexiform and nuclear layers, because these layers are proximal to NO-generating enzymes in microvessels and amacrine cells. On the other hand, external limiting membrane is located far from the NO-generating site.

Approaches for mechanistic probing of signal transduction by gases are going to unravel how multiple gases regulate cellular and tissue functions *in vivo*. Although physiologic roles of CO in neural tissues are unknown, retina could benefit from this nonradical sGC agonist to maintain housekeeping cyclic GMP without causing potential degradation of retinoids through a radical agonist such as NO. Such a way to utilize CO appears to be the case in stress-induced spermatogenic control or in relaxation of hepatic stellate cells for increasing sinusoidal blood flow where NO-breakable DNA or vitamin A is heavily stored, respectively (6, 21, 33). These findings enable a new understanding of the link between multiple gases and the function of transducers *in vivo*.

ACKNOWLEDGMENTS

The authors wish to acknowledge support by 21st Century Center-of-Excellence Program and by a grant for the 21st Century Leading Project for Biosimulation of Biological Systems from the Ministry of Education, Sciences and Technology of Japan. We thank Dr. Mayumi Kajimura for preparing photographs and figures.

ABBREVIATIONS

CO, carbon monoxide; DAF, diaminofluorescein; HO, heme oxygenase; mAb, monoclonal antibody; L-NAME; N^{ω}-nitro-L-arginine methyl ester; 7-NI, 7-nitroindazole; NO, nitric oxide; NOS, nitric oxide synthase; ROS, reactive oxygen species; sGC, soluble guanylate cyclase; SOD, superoxide dismutase.

REFERENCES

1. Bautista AP and Spitzer JJ. Inhibition of nitric oxide formation in vivo enhances superoxide release by the perfused liver. *Am J Physiol* 266: G783–G788, 1994.
2. Ellsworth ML, Forrester T, Ellis CG, and Dietrich HH. The erythrocyte as a regulator of vascular tone. *Am J Physiol* 269: H2155–H2161, 1995.
3. Fitzpatrick FA and Murphy RC. Cytochrome P450 metabolism of arachidonic acid: formation and biological actions of "epoxygenase"-derived eicosanoids. *Pharmacol Rev* 40: 229–241, 1989.
4. Friebe A, Schultz G, and Koesling D. Sensitizing soluble guanylate cyclase to become a highly CO-sensitive enzyme. *EMBO J* 15: 6863–6868, 1996.
5. Gaboury JP, Woodman RC, Granger DN, Reinhardt P, and Kubes P. Nitric oxide prevents leukocyte adherence: role of superoxide. *Am J Physiol* 265: H862–H867, 1993.
6. Goda N, Suzuki K, Naito M, Takeoka S, Tsuchida E, Ishimura Y, Tamatani T, and Suematsu M. Distribution of heme oxygenase isoforms in rat liver: topographic basis

for carbon monoxide-mediated microvascular relaxation. *J Clin Invest* 101: 604–612, 1998.
7. Gow AJ, Chen Q, Hess DT, Day BJ, Ischiropoulos H, and Stamler JS. Basal and stimulated protein *S*-nitrosylation in multiple cell types and tissues. *J Biol Chem* 277: 9637–9640, 2002.
8. Hayashi S, Takamiya R, Yamaguchi T, Matsumoto K, Tojo SJ, Tamatani T, Kitajima M, Makino N, Ishimura Y, and Suematsu M. Induction of heme oxygenase-1 suppresses venular leukocyte adhesion elicited by oxidative stress: role of bilirubin generated by the enzyme. *Circ Res* 85: 663–671, 1999.
9. Imai T, Morita T, Shindo T, Nagai R, Yazaki Y, Kurihara H, Suematsu M, and Katayama S. Vascular smooth muscle cell-directed overexpression of heme oxygenase-1 elevates blood pressure through attenuation of nitric oxide-induced vasodilation in mice. *Circ Res* 89: 55–62, 2001.
10. Intaglietta M, Johnson PC, and Winslow RM. Microvascular and tissue oxygen distribution. *Cardiovasc Res* 32: 632–643, 1996.
11. Kajimura M, Shimoyama M, Tsuyama S, Suzuki T, Kozaki S, Takenaka S, Tsubota K, Oguchi Y, and Suematsu M. Visualization of gaseous monoxide reception by soluble guanylate cyclase in the rat retina. *FASEB J* 17: 506–508, 2003.
12. Kashiwagi S, Kajimura M, Yoshimura Y, and Suematsu M. Nonendothelial source of nitric oxide in arterioles but not in venules: alternative source revealed in vivo by diaminofluorescein microfluorography. *Circ Res* 91: e55-e64, 2002.
13. Kawada N, Tran-Thi TA, Klein H, and Decker K. The contraction of hepatic stellate (Ito) cells stimulated with vasoactive substances: possible involvement of endothelin 1 and nitric oxide in the regulation of the sinusoidal tonus. *Eur J Biochem* 213: 815–823, 1993.
14. Koesling D and Friebe A. Soluble guanylate cyclase: structure and regulation. *Rev Physiol Biochem Pharmacol* 135: 41–65, 1999.
15. Kojima H, Nakatsubo N, Kikuchi K, Kawahara S, Kirino Y, Nagoshi H, Hirata Y, and Nagano T. Detection and imaging of nitric oxide with novel fluorescent indicators: diaminofluoresceins. *Anal Biochem* 70: 2446–2453, 1998.
16. Kubes P, Suzuki M, and Granger DN. Nitric oxide: an endogenous modulator of leukocyte adhesion. *Proc Natl Acad Sci USA* 88: 4651–4655, 1991.
17. Kubes P, Kanwar S, Niu XF, and Gaboury JP. Nitric oxide synthesis inhibition induces leukocyte adhesion via superoxide and mast cells. *FASEB J* 7: 1293–1299, 1993.
18. Kyokane T, Norimizu S, Taniai H, Yamaguchi T, Takeoka S, Tsuchida E, Naito M, Nimura Y, Ishimura Y, and Suematsu M. Carbon monoxide from heme catabolism protects against hepatobiliary dysfunction in endotoxin-treated rat liver. *Gastroenterology* 120: 1227–1240, 2001.
19. Moncada S, Palmer RMJ, and Higgs EA. Nitric oxide: physiology, pathophysiology and pharmacology. *Pharmacol Rev* 43: 109–142, 1991.
20. Morisaki H, Katayama T, Kotake Y, Ito M, Tamatani T, Sakamoto S, Ishimura Y, Takeda J, and Suematsu M. Roles of carbon monoxide in leukocyte and platelet dynamics in rat mesentery during sevoflurane anesthesia. *Anesthesiology* 95: 192–199, 2001.
21. Ozawa N, Goda N, Makino N, Yamaguchi T, Yoshimura Y, and Suematsu M. Leydig cell-derived heme oxygenase-1 regulates apoptosis of premeiotic germ cells in response to stress. *J Clin Invest* 109: 457–467, 2002.
22. Patel KD, Zimmerman GA, Prescott SM, McEver RP, and McIntyre TM. Oxygen radicals induce human endothelial cells to express GMP-140 and bind neutrophils. *J Cell Biol* 112: 749–759, 1991.
23. Stamler JS, Jia L, Eu JP, McMahon TJ, Demchenko IT, Bonaventura J, Gernert K, and Piantadosi CA. Blood flow regulation by *S*-nitrosohemoglobin in the physiological oxygen gradient. *Science* 276: 2034–2037, 1997.
24. Suematsu M. In vivo visualization of oxidative stress during endothelium-leukocyte interactions in endotoxemic rats. *J Jpn Coll Angiol* 31: 339–346, 1990 (in Japanese).
25. Suematsu M. Gas biology: how do the gases conduct protein function in vivo? *Seikagaku* 74: 1317–1328, 2002 (in Japanese).
26. Suematsu M and Ishimura Y. The heme oxygenase–carbon monoxide system: a regulator of hepatobiliary function. *Hepatology* 31: 3–6, 2000.
27. Suematsu M and Tsuchiya M. Platelet-activating factor and granulocyte-mediated oxidative stess: strategy for in vivo oxyradical visualization. *Lipids* 26: 1362–1368, 1991.
28. Suematsu M, Oshio C, Miura S, and Tsuchiya M. Real-time visualization of oxyradical burst from single neutrophil by using ultrasensitive video intensifier microscopy. *Biochem Biophys Res Commun* 149: 1106–1110, 1987.
29. Suematsu M, Oshio C, Miura S, Suzuki M, Houzawa S, and Tsuchiya M. Luminol-dependent photoemission from single neutrophil stimulated by phorbol ester and calcium ionophore: role of degranulation and myeloperoxidase. *Biochem Biophys Res Commun* 155: 106–111, 1988.
30. Suematsu M, Kurose I, Asako H, Miura S, and Tsuchiya M. In vivo visualization of oxyradical-dependent photoemission during endothelium-granulocyte interaction in microvascular beds treated with platelet activating factor. *J Biochem (Tokyo)* 106: 355–360, 1989.
31. Suematsu M, Tamatani T, DeLano FA, Miyasaka M, Forrest M, Suzuki H, and Schmid-Schoenbein GW. Microvascular oxidative stess preceding leukocyte activation elicited by in vivo nitric oxide suppression. *Am J Physiol* 266: H2410–H2415, 1994.
32. Suematsu M, Kashiwagi S, Sano T, Goda N, Shinoda Y, and Ishimura Y. Carbon monoxide as an endogenous modulator of hepatic vascular perfusion. *Biochem Biophys Res Commun* 205: 1333–1337, 1994.
33. Suematsu M, Goda N, Sano T, Kashiwagi S, Egawa T, Shinoda Y, and Ishimura Y. Carbon monoxide: an endoge-

nous modulator of sinusoidal tone in the perfused rat liver. *J Clin Invest* 96: 2431–2437, 1995.
34. Suzuki H, Suematsu M, Miura S, Liu YY, Watanabe K, Miyasaka M, Tsurufuji S, and Tsuchiya M. Rat CINC/gro: a novel mediator for locomotive and secretagogue activation of neutrophils in vivo. *J Leukoc Biol* 55: 652–657, 1994.
35. Suzuki M, Inauen W, Kvietys PR, Grisham MB, Meininger C, Schelling ME, Granger HJ, and Granger DN. Superoxide mediates reperfusion-induced leukocyte–endothelial cell interactions. *Am J Physiol Heart Circ Physiol* 257: H1740– H1745, 1989.
36. Takamiya R, Murakami M, Kajimura M, Goda N, Makino N, Takamiya Y, Yamaguchi T, Ishimura Y, Hozumi N, and Suematsu M. Stabilization of mast cells by heme oxygenase-1: an anti-inflammatory role. *Am J Physiol Heart Circ Physiol* 283: H861–H870, 2002.
37. Urakami-Harasawa L, Shimokawa H, Nakashima M, Egashira K, and Takeshita A. Importance of endothelium-derived hyperpolarizing factor in human arteries. J Clin Invest 100: 2793–2799, 1997.
38. Weiss SJ. Tissue destruction by neutrophils. *N Engl J Med* 320: 365–376, 1989.
39. Willis D, Moore AR, Frederick R, and Willoughby DA. Heme oxygenase: a novel target for the modulation of the inflammatory response. *Nat Med* 2: 87–89, 1996.
40. Yonetani T, Tsuneshige A, Zhou Y, and Chen X. Electron paramagnetic resonance and oxygen-binding studies of α-nitrosyl hemoglobin: a novel oxygen carrier having NO-assisted allosteric functions. *J Biol Chem* 273: 20323–20333, 1998.

Address reprint requests to:
Makoto Suematsu, M.D., Ph.D.
Professor and Chair
Department of Biochemistry and Integrative Medical Biology
School of Medicine, Keio University
35 Shinanomachi, Shinjuku-ku
Tokyo 160-8582, Japan

E-mail: msuem@sc.itc.keio.ac.jp

Received for publication December 27, 2002; accepted March 19, 2003.

Free Radical Biology & Medicine, Vol. 34, No. 12, pp. 1621–1630, 2003

0891-5849/03/$–see front matter

ELSEVIER

doi:10.1016/S0891-5849(03)00218-1

Original Contribution

SUPPRESSED APOPTOSIS IN THE INFLAMED GASTRIC MUCOSA OF *HELICOBACTER PYLORI*-COLONIZED iNOS-KNOCKOUT MICE

MASAHARU MIYAZAWA,* HIDEKAZU SUZUKI,* TATSUHIRO MASAOKA,* AKEMI KAI,‡ MAKOTO SUEMATSU,§ HIROSHI NAGATA,* SOICHIRO MIURA,† and HIROMASA ISHII*

Departments of *Internal Medicine and †Biochemistry and Integrative Medical Biology, Keio University School of Medicine, Tokyo, Japan; ‡2nd Department of Internal Medicine, National Defense Medical College, Tokorozawa, Japan; and §Tokyo Metropolitan Research Laboratory of Public Health, Tokyo, Japan

(*Received* 9 *January* 2003; *Revised* 24 *March* 2003; *Accepted* 28 *March* 2003)

Abstract—Deregulated cell turnover in *Helicobacter pylori* (*H. pylori*)-colonized gastric mucosa has been suggested to be linked to the gastric carcinogenesis pathway. We previously reported attenuation of apoptosis and enhancement of cellular proliferation in the *H. pylori*-colonized gastric mucosa of Mongolian gerbils as compared to that in mice, which might reflect a specific link between *H. pylori* colonization and carcinogenesis in the Mongolian gerbils; the difference between the two strains could be attributable to differences in the host genetic background. Inducible-type nitric oxide synthase (iNOS) is thought to participate in not only the inflammatory response, but also in the regulation of gastric mucosal cell turnover in *H. pylori*-colonized gastric mucosa. Thus, the present study was designed to examine gastric leukocyte activation and epithelial cell apoptosis in the gastric mucosa following *H. pylori* inoculation in iNOS-knockout mice. Methods: iNOS-knockout mice ($iNOS^{-/-}$) and their $iNOS^{+/+}$ littermates were orally inoculated with the Sydney strain of *H. pylori* (SS1, 10^8 colony-forming units [CFU]). *H. pylori* infection was confirmed by microaerobic bacterial culture. The stomach of each mouse was evaluated 14 weeks and 30 weeks after the inoculation. Gastric mucosal accumulation of polymorphonuclear leukocytes (PMN) was assessed by determining the myeloperoxidase (MPO) activity and histological score based on the updated Sydney system. The level of apoptosis was determined by estimation of the cytoplasmic levels of mono- and oligonucleosomes and by the terminal deoxynucleotidyl transferase-mediated deoxyuridine triphosphate nick-end labeling method. Results: The SS1-inoculated mice showed persistent *H. pylori* colonization for 12 weeks. While gastric mucosal PMN infiltration increased following SS1 inoculation in both $iNOS^{+/+}$ and $iNOS^{-/-}$ strains, enhanced DNA fragmentation was observed in only SS1-colonized $iNOS^{+/+}$ mice, and not in the $iNOS^{-/-}$ mice. In conclusion, although the recruitment of PMN in response to *H. pylori* was evoked even in the gastric mucosa of $iNOS^{-/-}$ mice, epithelial cell apoptosis induced by *H. pylori* was attenuated in this strain. These data suggest that iNOS may play an important role in promoting apoptosis in the *H. pylori*-infected inflamed gastric mucosa, and that persistent inflammation without apoptosis in $iNOS^{-/-}$ mice with *H. pylori* infection may be linked to preneoplastic transformation. © 2003 Elsevier Inc.

Keywords—Nitric oxide, Myeloperoxidase, Leukocyte, Oligonucleosome

INTRODUCTION

Helicobacter pylori is now widely recognized as one of the major causative agents of gastritis and peptic ulcer disease. However, in regard to the link between the development of gastric cancer and *H. pylori* infection, numerous issues remain unresolved. Recently, Uemura et al. [1] reported, based on a large-scale, long-term endoscopic follow-up study, that gastric-intestinal type carcinoma developed only in *H. pylori*-positive cohorts. On the other hand, Japanese researchers [2,3] have succeeded in inducing gastric cancer by inoculating only Mongolian gerbils with *H. pylori*. According to their reports, intestinal-type gastric adenocarcinoma developed in about one third of the gerbils 72–90 weeks after the bacterial inoculation. However, no such cancer development occurred in smaller animals, such as mice, following *H. pylori* inoculation. We previously compared the levels of epithelial cell apoptosis and proliferation

Address correspondence to: Hidekazu Suzuki, M.D., Ph.D., Department of Internal Medicine, Keio University School of Medicine, 35 Shinanomachi, Shinjuku-ku, Tokyo 160-8582, Japan; Tel: +81 (3) 5363-3914; Fax: +81 (3) 5363-3967; E-Mail: hsuzuki@sc.itc.keio.ac.jp.

of gastric mucosal cells in *H. pylori*-colonized gastric mucosa between Mongolian gerbils and C57BL/6 mice, and demonstrated attenuated apoptosis and enhanced mucosal cell proliferation only in the gerbils, possibly reflective of a specific link between *H. pylori* infection and carcinogenesis in Mongolian gerbils. It was suggested that the difference between the two strains might be due to differences in the host genetic background [4]. In other words, the factor responsible for the attenuated epithelial cell apoptosis in the inflamed gastric mucosa of mice might also be linked to the increased tendency towards carcinogenesis observed in Mongolian gerbils.

Levels of inducible nitric oxide synthase (iNOS) have been reported to be enhanced in *H. pylori*-colonized gastric mucosa [5]. According to the report by Li et al. [6], higher levels of both oxidized and nitrated proteins were found in patients with either chronic gastritis or duodenal ulcer than in those with normal gastric mucosa. The levels of modified proteins were significantly higher in inflamed tissues infected with *H. pylori*, and in those showing positive expression of IL-8 and iNOS mRNA as compared to those negative for these parameters [6]. These findings suggest that *H. pylori* infection induces significant oxidative stress and iNOS expression in the gastric mucosa, presumably contributing to the pathogenesis of *H. pylori*-associated gastroduodenal diseases.

The in vitro cytotoxicity of *H. pylori* in combination with proinflammatory cytokines was inhibited by iNOS suppression [7], suggesting a potent role of iNOS and its derivatives in gastric cellular apoptosis. These results raise the possibility of apoptosis inhibition via iNOS suppression in vivo in mice.

Thus, the present study was designed to examine the extent of gastric leukocyte activation and epithelial cell apoptosis following *H. pylori* inoculation in the gastric mucosa of iNOS-knockout mice.

MATERIALS AND METHODS

Animal Procedure

All experiments and procedures carried out on the animals were approved by the Keio University Animal Research Committee (No.001022). Seven week old, specific-pathogen-free male iNOS-knockout mice ($iNOS^{-/-}$; B6.129P2-NOS2, The Jackson Laboratory, Bar Harbor, ME, USA) and the corresponding control ($iNOS^{+/+}$) mice were used for the study. The Sydney strain of *H. pylori* (SS1) for each challenge was grown from frozen stocks at 37°C under microaerobic conditions for 24–36 h on lysed horse blood agar supplemented with antibiotics, harvested in brucella broth, and administered to the animals immediately after harvesting. Fourteen $iNOS^{-/-}$ mice and 9 wild-type $iNOS^{+/+}$ mice were administered suspensions of SS1 (5×10^8 CFU/ml, 15 ml/kg, ×2), while a further 13 $iNOS^{-/-}$ mice and 10 $iNOS^{+/+}$ mice were administered suspensions of buffer solution alone after overnight starvation. All animals appeared to be alert and in good health after the inoculation. Two weeks later, the animals were inoculated again with the aforementioned bacterial strain. Fourteen weeks later, 6 $iNOS^{-/-}$ control mice and 5 $iNOS^{+/+}$ control mice, and 7 $iNOS^{-/-}$ mice and 5 $iNOS^{+/+}$ mice from the *H. pylori*-infected group were sacrificed for examination. Then again, 30 weeks after the inoculation, 7 $iNOS^{-/-}$ mice and 5 $iNOS^{+/+}$ mice from the control group, and 7 $iNOS^{-/-}$ mice and 4 $iNOS^{+/+}$ mice from the *H. pylori*-inoculated group were sacrificed for examination (Fig. 1). The excised stomachs were cut along the greater curvature and rinsed with physiological saline [8].

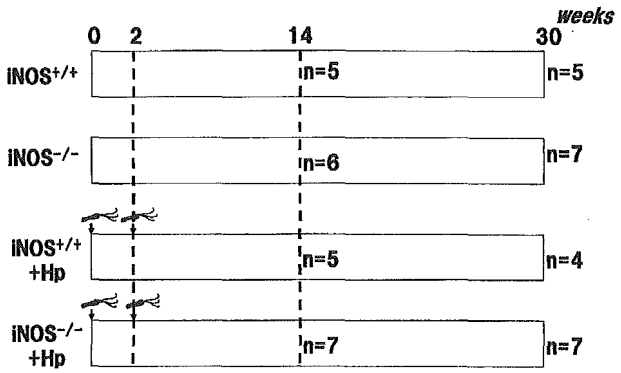

Fig. 1. Experimental protocol for each animal group.

Microaerobic bacterial culture of H. pylori

H. pylori infection at each time-point was evaluated by counting the number of CFUs following microaerobic bacterial culture. The stomachs were homogenized in 20 ml of phosphate-buffered saline (PBS) using a Polytron (Kinematica, Steinhofhalde, Switzerland). The diluted homogenates were inoculated on to Brucella agar (Invitrogen, Groningen, The Netherlands) plates containing 10% horse blood (Nippon Bio-Test, Tokyo, Japan), 2.5 μg/ml of amphotericin B, 9 μg/ml of vancomycin, 0.32 μg/ml of polymyxin B, 5 μg/ml of trimethoprim, and 50 μg/ml of 2, 3, 5-triphenyl-tetrazolium chloride. The plates were then incubated at 37°C in a microaerobic atmosphere for 7 d. Colonies were counted, and the amount of viable *H. pylori* was expressed as CFU per gram of tissue [9].

Measurement of plasma nitrates and nitrites

Plasma NOX (nitrates and nitrites) was measured using a modification of a previously described assay method [10]. Briefly, 100 μl from each plasma sample

were incubated (37°C) for 30 min in 0.05 M N-[2-hydroxyethyl]piperazine-N'-[2-ethanesulfonic acid] buffer (pH 7.4) containing 5 mM flavin adenine dinucleotide (FAD), 100 mM reduced nicotinamide adenine dinucleotide phosphate (NADPH), and 10 U/ml nitrate reductase (Boehringer Mannheim, Indianapolis, IN, USA). Lactate dehydrogenase (1,500 U/ml, Sigma-Aldrich Japan K.K., Tokyo, Japan) and 0.01 M sodium pyruvate (Sigma-Aldrich Japan K.K.) were added to each tube, and the incubation was continued for 10 min. The Griess reagent was then added, and after 10 min, the nitrite content was determined colorimetrically at 543 nm.

MPO activity

Tissue samples of gastric mucosa were homogenized with 1.5 ml of 10 mM potassium phosphate buffer (pH 7.8) containing 30 mM KCl in a Teflon homogenizer. The homogenate was then sonicated over ice in 30 consecutive 0.5 s bursts at 0.5 s intervals, at a power setting of 60 W (Sonifier Cell Disruptor Model 185, Branson, Shelton, CT, USA). The total protein content in the homogenates was measured by modified Lowry's method [11], as described by Smith et al. [12]. Myeloperoxidase (MPO) activity, an index of tissue-associated neutrophil accumulation, was determined by a modification of Grisham et al.'s method [13]. One hundred microliter samples of mucosal homogenates were centrifuged at 8000 × *g* for 15 min at 4°C to separate the pellets of insoluble cellular debris. The pellets were rehomogenized in an equal volume of 0.05 M potassium phosphate buffer (pH 5.4) containing 0.5%-hexadecyltrimethylammonium bromide. The samples were then centrifuged at 8000 × *g* for 15 min at 4°C and the supernatants were reserved. MPO activity in the supernatants was assessed by measuring the H_2O_2-dependent oxidation of 3,3',5,5'-tetramethylbenzidine. One unit of enzyme activity was defined as the amount of MPO that caused a change in absorbance of 1.0/min at 655 nm, at 25°C.

Assay for cytoplasmic mono- and oligonucleosomes

DNA fragmentation in the epithelial cells was evaluated by photometric enzyme immunoassay to determine the cytoplasmic levels of mono- and oligonucleosomes (histone-associated DNA fragments) (Boehringer Mannheim GmbH, Mannheim, Germany). Briefly, gastric mucosal tissue specimens from mice were incubated at 37°C for 2 h in the lysis buffer. The tissue lysates were then centrifuged at 8000 × *g* for 15 min at 4°C, and the supernatants were transferred into a streptavidin-precoated 96 well microplate. Biotinylated antihistone antibody, which binds to histone H1, H2A, H2B, H3, or H4, and peroxidase-labeled anti-DNA antibody were then added. Two hours later, the supernatants were removed and incubated with the substrate solutions. The absorbances (at 405 nm) were measured with a microplate reader (Bio-Rad Laboratories, Inc., Hercules, CA, USA) [4]. The apoptosis index was computed according to the following equation:

$$\text{Apoptosis index (\%)} = (Ax - An)/(Ap - An) \times 100,$$

where *Ax* indicates the absorbance value at 405 nm of each test solution, *Ap* indicates the absorbance value at 405 nm of the positive control, and *An* indicates the absorbance value at 405 nm of the negative control.

Histological examination

Portions of gastric tissue samples were fixed in 10%-neutralized formalin and embedded in paraffin. Then, 4 to 6 μm paraffin sections were placed on slides pretreated with a 0.01% aqueous solution of poly-l-lysine. Deparaffinization was achieved by heating the sections for 10 min at 70°C. Hydration involved passing the slides through the following solutions: twice in a xylene bath for 5 min each, and then twice each for 3 min in 96% ethanol and 90% ethanol, and finally in double-distilled water.

Several thin sections of fixed tissue were stained with hematoxylin and eosin for visualization of the polymorphonuclear and mononuclear infiltration. All the sections were reviewed by a single histopathologist who was unaware of the other findings. Polymorphonuclear cell and mononuclear cell infiltration was graded as follows: 0 = minimal, 1 = mild, 2 = moderate, and 3 = severe, according to the updated Sydney system [14], a modification of the original Sydney system [15,16].

TUNEL (terminal deoxynucleotidyl transferase-mediated deoxyuridine triphosphate nick-end labeling)

The nuclei of the tissue sections were stripped of proteins by incubation with 10 μg/ml proteinase K (PK) (Sigma-Aldrich Japan K.K.) for 15 min at room temperature, and the slides were then washed four times in distilled water for 2 min each. Endogenous peroxidase was inactivated by covering the sections with 2% H_2O_2 for 5 min at room temperature. The sections were rinsed with distilled water, and immersed in TDT buffer (25 mM Tris-HCl, pH 6.5, 200 mM potassium cacodylate, 1 mM cobalt chloride, 0.25 mg/ml bovine serum albumin [BSA]). TDT (200 U/ml, Takara Bio Inc., Ootsu, Japan) and biotinylated dUTP (0.01 mM, Dako Japan Co., Ltd., Kyoto, Japan) in TDT buffer were then added to cover the sections, followed by incubation in a humid atmosphere at 37°C for 60 min. The reaction was terminated

by transferring the slides to TB buffer (300 mM sodium chloride, 30 mM sodium citrate) for 15 min at room temperature. The sections were rinsed with distilled water, covered with a 2% aqueous solution of BSA for 10 min at room temperature, rinsed in distilled water, and immersed in PBS for 5 min. They were then covered with an enzyme solution supplied by a streptavidin horse radish peroxidase (HRP) detection system (Invitrogen Corp., Carlsbad, CA, USA) for 45 min. The slides were then washed with 0.02 M PBS containing 0.15 M NaCl and incubated with 0.02% 3,3'-diaminobentidine tetrahydrochloride (DAB) colorimetric solution [17]. After rinsing in distilled water, they were stained with Mayer hematoxylin solution for about 30 min at 37°C. The specimens were quickly dehydrated in 95% ethanol, twice in 100% ethanol and twice in xylene. The tissue sections were then mounted in Permount (Fisher Scientific, Pittsburgh, PA, USA).

Apoptotic cells identified by TUNEL assay were quantitated under brightfield microscopy by a single observer blinded to the *H. pylori* infection and animal status. The cell number in six different high-power fields was counted for each specimen (40× objective).

PCNA- positive cells

The slides were placed in 10 mM preheated citrate buffer for 30 min. After being washed in PBS, the tissue sections were incubated for 10 min in a solution used for blocking nonspecific reactions (Dako Japan). The sections were then incubated with the primary antibody against proliferating cell nuclear antigen (PCNA; antihuman, cross-reacts with mouse, immunoglobulin G2a subclass; Pharmingen, San Diego, CA, USA) at a 1:1500 dilution for 60 min at room temperature, using the avidin-biotin method, in combination with HRP. After rinsing, the slides were incubated with a secondary biotinylated antibody provided in the ABC kit (Vectastain Elite ABC Kit; Vector Laboratories, Burlingame, CA, USA) for 30 min at room temperature, then with the streptavidin-HRP complex provided in the ABC kit for 30 min at room temperature. After rinsing again, the slides were developed in DAB reagent (10 mg DAB in 10 ml of 0.5 M Tris buffer, 3 drops of 3% H_2O_2); each incubation step was followed by three washes (5 min each) in buffer (0.05 M Tris-HCl, 0.15 M NaCl, pH 7.6) [18]. Mayer hematoxylin solution was used for 30 min to counterstain the tissue sections. Dehydration was performed quickly in 95% ethanol, twice in 100% ethanol, and twice in xylene. The tissue sections were then mounted in Permount (Fisher Scientific). A single observer blinded to the *H. pylori* infection status quantified the extent of gastric epithelial cell proliferation by immunohistochemical staining for PCNA. The percentage of PCNA-positive cells (%) was determined by counting the number of PCNA-positive cells among the total number of epithelial cells in a high-power microscopic field [19].

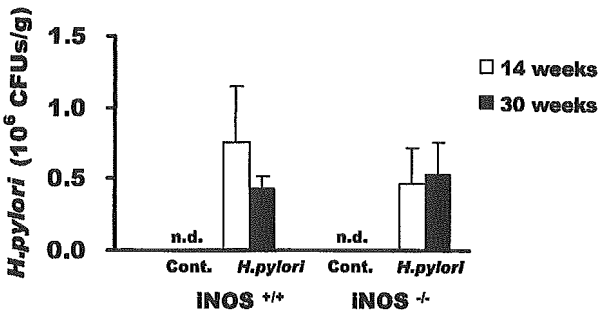

Fig. 2. The level of *Helicobacter pylori* colonization assessed by counting the number of colony forming units (CFUs) after microaerobic bacterial cultivation. n.d. = no colonies were detected following microaerobic *H. pylori* cultivation.

Statistical analysis

Data indicate mean values ± SEM. Statistical analysis was performed using analysis of variance and the results were compared with those obtained using Scheffe's test. A p value of $<.05$ was considered significant.

RESULTS

Fourteen weeks and 30 weeks after the inoculation, the number of CFUs of *H. pylori* counted after microaerobic *H. pylori* cultivation of the mouse gastric mucosa indicated persistent colonization of the stomach mucosa of both *H. pylori*-inoculated iNOS$^{-/-}$ and iNOS$^{+/+}$ mice with this bacterium. There was no significant difference in the levels of bacterial colonization between *H. pylori*-inoculated iNOS$^{-/-}$ and iNOS$^{+/+}$ mice either at 14 or 30 weeks (Fig. 2).

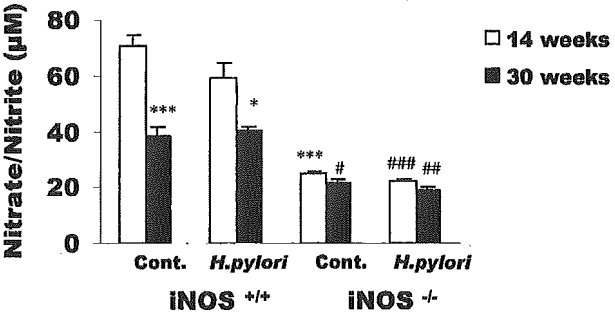

Fig. 3. The plasma level of nitrate/nitrite (NOx). ***$p < .001$ compared with that in the iNOS$^{+/+}$ control mice at 14 weeks. *$p < .05$ compared with that in the *Helicobacter pylori*-colonized iNOS$^{+/+}$ mice at 14 weeks. #$p < .05$ compared with that in the iNOS$^{+/+}$ control mice at 30 weeks. ###$p < .001$ compared with that in the *H. pylori*-infected iNOS$^{+/+}$ mice at 14 weeks. ##$p < .01$ compared with that in the *H. pylori*-infected iNOS$^{+/+}$ mice at 30 weeks.

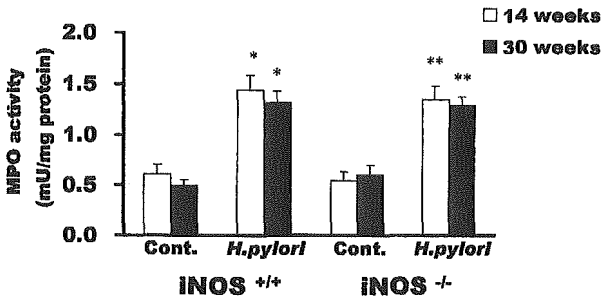

Fig. 4. Myeloperoxidase (MPO) activity in the gastric mucosa. *$p <$ .05 compared with that in the iNOS$^{+/+}$ control mice in each period at each time point. **$p <$ .01 compared with that in the iNOS$^{-/-}$ control mice in each period at each time point.

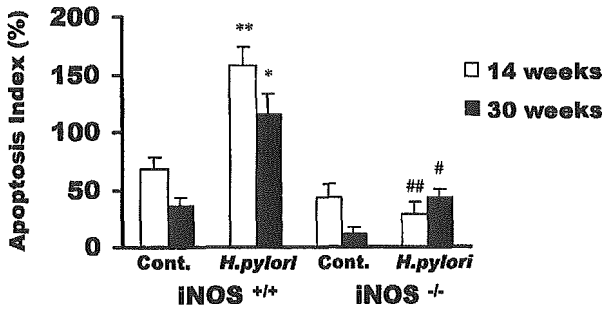

Fig. 5. Gastric mucosal apoptosis index (%) computed from the cytoplasmic contents of mono- and oligonucleosomes. **$p <$ .01 compared with that in the iNOS$^{+/+}$ control mice at 14 weeks. *$p <$ .05 compared with that in the iNOS$^{+/+}$ control mice at 30 weeks. ##$p <$ .01 compared with that in the *Helicobacter pylori*-infected iNOS$^{+/+}$ mice at 14 weeks. #$p <$ .05 compared with that in the *H. pylori*-infected iNOS$^{+/+}$ mice at 30 weeks.

Figure 3 shows the plasma levels of NOx. Although the mean NOx level was significantly higher in the control and *H. pylori*-colonized iNOS$^{+/+}$ mice at 14 weeks than at 30 weeks, and in the iNOS$^{+/+}$ mice of either group than in the iNOS$^{-/-}$ mice, no significant difference was observed between the control and *H. pylori*-infected cohorts. These results suggest that although iNOS$^{-/-}$ mice showed lower plasma levels of NOx, possibly due to the lack of iNOS-derived NO, the plasma level of NOx could not reflect the extent of local *H. pylori* colonization in the mice.

Figure 4 shows the MPO activity in the gastric mucosa. MPO activity was significantly increased in *H. pylori*-colonized mice, without any significant difference between iNOS$^{+/+}$ and iNOS$^{-/-}$ mice. These results demonstrate that the extent of *H. pylori* colonization and the associated leukocyte accumulation in the gastric mucosa occur to the same extent in iNOS$^{-/-}$ mice and iNOS$^{+/+}$ mice. These results were also confirmed by histological scoring according to the updated Sydney system for PMN cell infiltration (Table 1).

The score for mononuclear cell infiltration was also determined in tissue specimens (Table 1). The level of mononuclear cell infiltration was significantly increased in *H. pylori*-colonized mice, and there was no significant difference between iNOS$^{+/+}$ and iNOS$^{-/-}$ mice.

Figure 5 presents the gastric mucosal apoptosis index (%) as represented by the cytoplasmic contents of mono- and oligonucleosomes. Although the apoptosis index (%) was significantly increased in the iNOS$^{+/+}$ mice at 14 weeks after the bacterial inoculation, there was no significant increase in the iNOS$^{-/-}$ mice even after *H. pylori* colonization.

As represented in Fig. 6, a significantly large number of TUNEL-positive cells was observed in the surface epithelium of the gastric corpus mucosa of iNOS$^{+/+}$ mice with *H. pylori* colonization 14 weeks after the inoculation (Fig. 6b). However, the number of TUNEL-positive cells was significantly lower in the gastric mucosa of iNOS$^{-/-}$ mice, even in those showing *H. pylori* colonization 14 weeks after the inoculation (Fig. 6d), as compared with that in the gastric mucosa of iNOS$^{+/+}$ mice showing *H. pylori* colonization. The number of TUNEL-positive cells (%) in the tissue specimens was

Table 1. Histological Scores for Polymorphonuclear Cell (PMN) and Mononuclear Cell Infiltration

	Scores for PMN Infiltration				Scores for Mononuclear Cell Infiltration			
	iNOS$^{+/+}$		iNOS$^{-/-}$		iNOS$^{+/+}$		iNOS$^{-/-}$	
	Control	*H. pylori*	Control	*H. pylori*	Control	*H. pylori*	Control	*H. pylori*
14 weeks	0.40 ± 0.17	1.04 ± 0.18*	0.43 ± 0.12	1.20 ± 0.21‡	0.09 ± 0.04	0.63 ± 0.21*	0.05 ± 0.04	0.83 ± 0.13‖
30 weeks	0.44 ± 0.10	0.95 ± 0.22†	0.51 ± 0.10	1.00 ± 0.22§	0.09 ± 0.05	1.05 ± 0.15¶	0.31 ± 0.17	0.88 ± 0.25§

iNOS = inducible nitric oxide synthase, *H. pylori* = *helicobacter pylori*.
* $p <$ .05 compared with the iNOS$^{+/+}$ control mice at 14 weeks.
† $p <$ .05 compared with the iNOS$^{+/+}$ control mice at 30 weeks.
‡ $p <$ .01 compared with the iNOS$^{-/-}$ control mice at 14 weeks.
§ $p <$ .05 compared with the iNOS$^{-/-}$ control mice at 30 weeks.
¶ $p <$ .001 compared with the iNOS$^{+/+}$ control mice at 30 weeks.
‖ $p <$ .001 compared with the iNOS$^{-/-}$ control mice at 14 weeks.

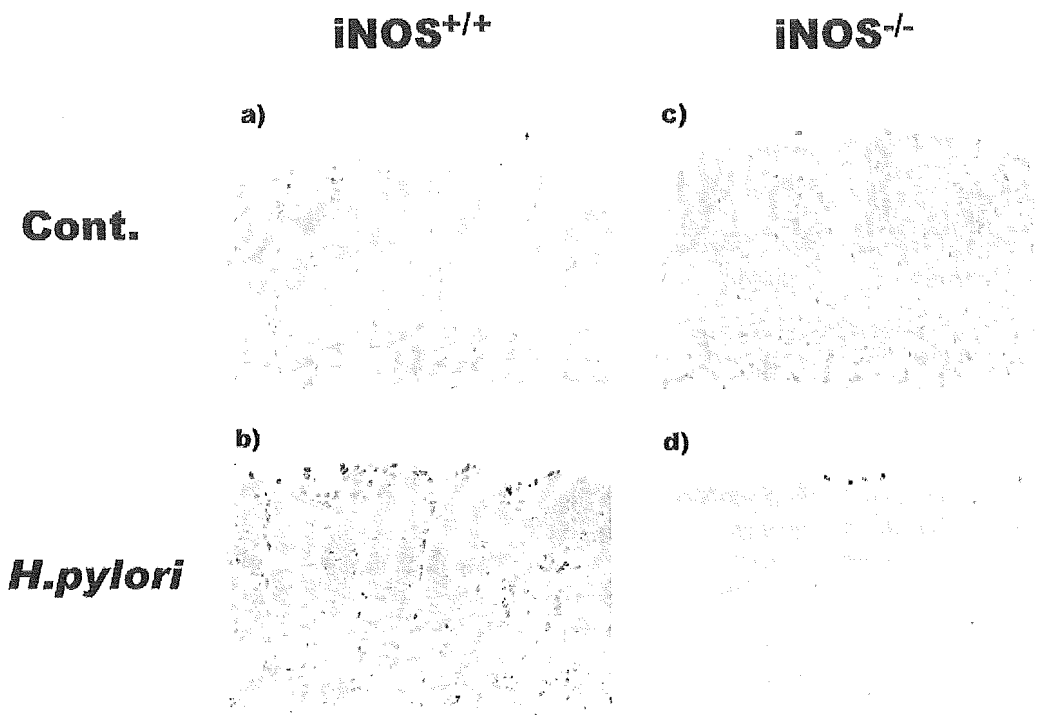

Fig. 6. Representative photomicrograph of terminal deoxynucleotidyl transferase-mediated deoxyuridine triphosphate nick-end labeling staining in the gastric corpus mucosa of mice at 14 weeks after the *H. pylori* inoculation. (a) Gastric corpus mucosa of the control iNOS$^{+/+}$ mouse. (b) Gastric corpus mucosa of the *H. pylori* colonized-iNOS$^{+/+}$ mouse. (c) Gastric corpus mucosa of the control iNOS$^{-/-}$ mouse. (d) Gastric corpus mucosa of the *H. pylori* colonized-iNOS$^{-/-}$ mouse. Objective lens: 40×.

also significantly increased in iNOS$^{+/+}$ mice 14 weeks and 30 weeks after the bacterial inoculation, but not in the iNOS$^{-/-}$ mice, even those showing *H. pylori* colonization (Fig. 7). These results suggest that gastric mucosal cell apoptosis in the *H. pylori*-colonized stomach mucosa is significantly attenuated in iNOS$^{-/-}$ mice. On the other hand, although the average number of TUNEL-positive cells (%) at 30 weeks was lower than that at 14 weeks after

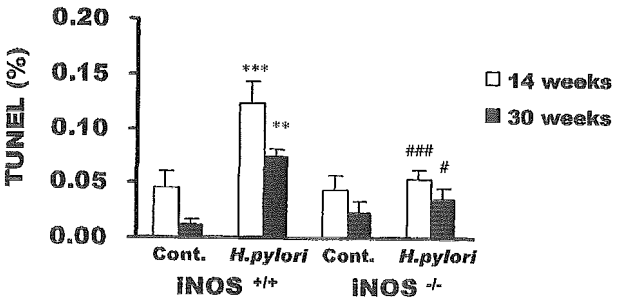

Fig. 7. Morphometric analysis for evaluation of gastric mucosal cell apoptosis expressed as terminal deoxynucleotidyl transferase-mediated deoxyuridine triphosphate nick-end labeling-positive cells (%). ***$p <$ .001 compared with that in the iNOS$^{+/+}$ control mice at 14 weeks. **$p <$ .01 compared with that in the iNOS$^{+/+}$ control mice at 30 weeks. ###$p <$ .001 compared with that in the *H. pylori*-infected iNOS$^{+/+}$ mice at 14 weeks. #$p <$ .05 compared with that in the *H. pylori*-infected iNOS$^{+/+}$ mice at 30 weeks.

H. pylori inoculation in the control and *H. pylori*-colonized iNOS$^{+/+}$ mice, there were no statistically significant differences in the number of TUNEL-positive cells (%) between 14 weeks and 30 weeks in the control and *H. pylori*-colonized iNOS$^{+/+}$ mice. This tendency towards decrease in the number of TUNEL-positive cells (%) with time might be due to the aging, that is, the turnover rate of gastric mucosal cells could be reduced and the detection rate of cells undergoing apoptosis might be reduced.

On the other hand, as shown in Fig. 8, PCNA-positive cells were observed in the upper-mid portion of the gastric mucosa in all the four different groups. The number of PCNA-positive cells did not differ significantly among the four different groups (Figs. 8a–d). Figure 9 shows the results of morphometric analysis of gastric mucosal cell proliferation, expressed as the percentage of PCNA-positive cells (%). Although the percentage of PCNA-positive cells (%) tended to be higher in the iNOS$^{-/-}$ mice, there were no significant differences in this parameter between the control and *H. pylori*-colonized mice, or between iNOS$^{+/+}$ and iNOS$^{-/-}$ mice.

DISCUSSION

The present study showed that the absence of iNOS expression was closely associated with attenuation of

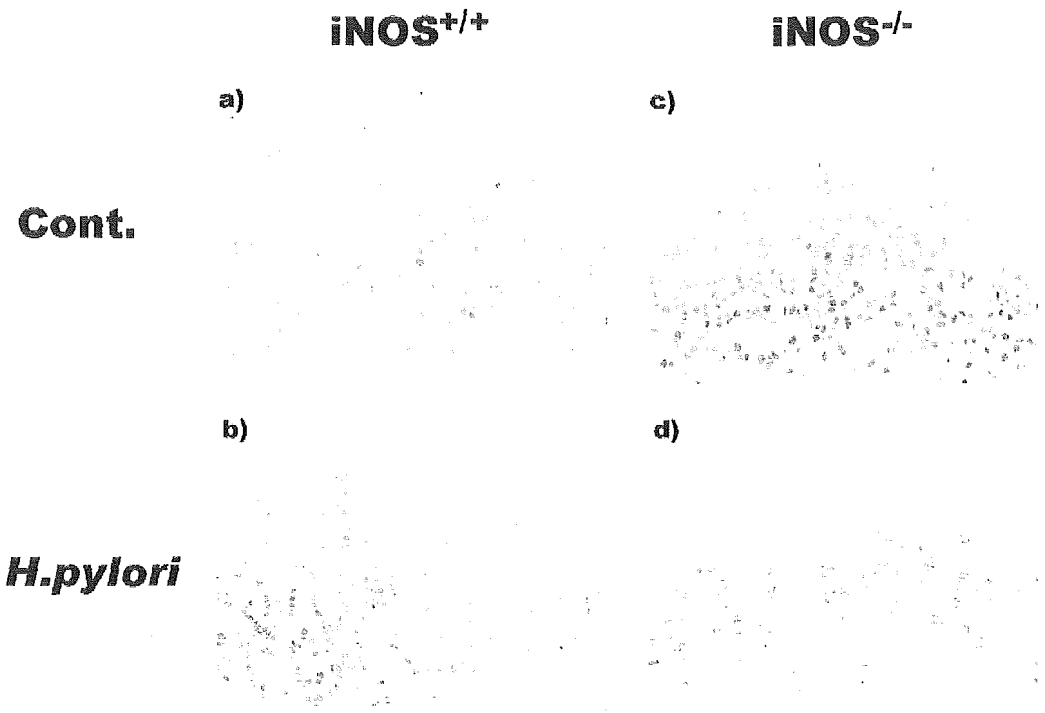

Fig. 8. Representative photomicrograph of proliferating cell nuclear antigen staining in the gastric corpus mucosa of mice at 14 weeks after the *Helicobacter pylori* inoculation. (a) Gastric corpus mucosa of the control iNOS$^{+/+}$ mouse. (b) Gastric corpus mucosa of the *H. pylori* colonized-iNOS$^{+/+}$ mouse. (c) Gastric corpus mucosa of the control iNOS$^{-/-}$ mouse. (d) Gastric corpus mucosa of the *H. pylori* colonized-iNOS$^{-/-}$ mouse. Objective lens: 40×.

cellular apoptosis in *H. pylori*-colonized inflamed gastric mucosa. In other words, an iNOS-derived oxidant (NO) might promote apoptosis in the *H. pylori*-colonized inflamed gastric mucosa and regulate healthy cell turnover.

Many investigators have reported that *H. pylori* infection increases the expression of iNOS mRNA and protein, both in vitro and in vivo [6,20–22]. We previously reported that iNOS and peroxinitrite expression increased in *H. pylori*-positive gastric mucosa of patients with gastric ulcer [5]. Although Kodama et al. [23] reported that the serum NOx concentrations in *H. pylori*-antibody-positive subjects were higher than those in the antibody-negative subjects, in the present study, the NOx levels did not increase after *H. pylori* colonization. Because the severity of gastric mucosal inflammation in *H. pylori*-colonized mice is usually lesser than that in humans with *H. pylori* infection, such a small enhancement of NO derived from the gastric mucosal iNOS might not significantly affect NOx concentration in the sera of mice.

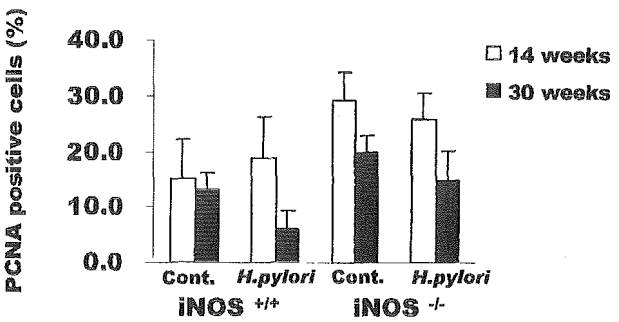

Fig. 9. Morphometric analysis for evaluation of gastric mucosal cell proliferation, expressed as a percentage of proliferating cell nuclear antigen (PCNA)-positive cells (%).

NO production in blood vessels, such as in isolated conduit arteries, has been reported to reduce with aging [24,25]. A decreased serum levels of nitric oxide precursor, L-arginine, and a decreased urinary excretion of metabolites, nitrate and nitrite, have been reported in aging rats [26]. Although the mechanisms for the reduced NOx level at 30 weeks in iNOS$^{+/+}$ mice could not be defined in this study, it might be explained by aging of the mice.

Peek et al. [27] investigated the level of gastric epithelial cell apoptosis and proliferation in the *H. pylori*-colonized gastric mucosa of Mongolian gerbils and demonstrated an initial transient enhancement of cellular apoptosis (2–4 weeks) and a later increase in cellular proliferation (16–20 weeks). We also previously reported that while gastric mucosal cell apoptosis in-

creased in parallel with the degree of *H. pylori*-evoked inflammation in C57BL/6 mice, the level of apoptosis was significantly attenuated in *H. pylori*-colonized gastric mucosa in Mongolian gerbils in association with an exacerbated inflammatory response and increased proliferation of gastric mucosal cells, in response to long-term colonization (36 and 72 weeks after the bacterial inoculation) [4]. These results suggested a possible link between attenuated gastric mucosal apoptosis and a specific carcinogenesis sequence in Mongolian gerbils with *H. pylori* colonization of the gastric mucosa [2,3]. The results of this study also suggest that the gastric mucosal regulator of apoptosis might play a key role in the genesis of gastric malignancy.

One of the suspected candidates involved in the regulation of apoptosis is *p53*. Mutations of the *p53* tumor suppressor gene constitute one of the most frequently encountered molecular changes in a wide variety of human cancers. Fox et al. [28] examined $p53^{+/-}$ mice inoculated with *Helicobacter felis* and observed a significant enhancement of gastric mucosal cell proliferation at 48 weeks after the inoculation as compared with that at the corresponding time-point in the stomachs of wild-type mice colonized by the same bacteria. In their report, mild to moderate nodular to plaque-like thickening of the mucosa with microscopically hypertrophic and hyperplastic mucosal epithelium was observed in the gastric corpus in both $p53^{+/-}$ and wild-type mice at 24 weeks after the inoculation. However, they did not describe the differences in the proliferative indices between $p53^{+/-}$ and wild-type mice at 24 weeks. We also reported [29], using the same $p53^{+/-}$ mice as those by Fox et al. [28], that there were no differences between the levels of cellular apoptosis and proliferation in the gastric mucosa at 24 weeks after *H. pylori* (not *H. felis*) inoculation between $p53^{+/-}$ and wild-type mice. Yamamoto et al. [30] investigated the susceptibility of *p53* nullizygote$^{-/-}$, heterozygote,$^{+/-}$ and wild-type$^{+/+}$ mice to N:-methyl-N:-nitrosourea-induced gastric carcinogenesis, and reported that gastric adenocarcinomas did not develop in $p53^{+/-}$ mice. These results suggest that heterozygous mutations of *p53* may not be sufficient to induce murine gastric preneoplastic and neoplastic lesions, even with the administration of a chemical carcinogen. These earlier reports suggest that an additional genetic change may be necessary to evoke deregulation of gastric mucosal cell turnover in *H. pylori*-colonized stomach mucosa.

According to our previous observations, the number of proliferating cells (PCNA-positive cells) in the gastric mucosa of *H. pylori*-colonized C57BL/6 mice was not significantly increased as compared with that in the gastric mucosa of control uncolonized mice at 72 weeks after bacterial inoculation [4]. Furthermore, also in the present study, there were no differences in the level of PCNA-positive cells (%) between $iNOS^{-/-}$ and $iNOS^{+/+}$ (C57BL/6) mice, or between *H. pylori*-colonized and non-*H. pylori*–colonized mice 14 and 30 weeks after the bacterial inoculation (Fig. 8). These data collectively indicate that *H. pylori* colonization in mice may not markedly alter the level of cellular proliferation in the gastric mucosa.

According to the report by Kiss et al. [31], significant increases in albumin leakage and the expression of iNOS in both antral and duodenal tissues of rats were observed following lipopolysaccharide (LPO) challenge, and concurrent administration of a selective iNOS inhibitor caused a dose-dependent attenuation of the gastric and duodenal albumin leakage. These findings suggest that iNOS expression is initiated by *H. pylori* LPS, with consequent increase in the gastric and duodenal microvascular permeability. Recently, Watanabe et al. [7] found in an in vitro study, that chemical iNOS suppression by aminoguanidine attenuated *H. pylori*-induced apoptosis of MKN45 cells, suggesting an important role of iNOS-associated factors in evoking cellular apoptosis in the gastric mucosa.

NO may be tumoricidal, and has been shown to have the ability to induce apoptosis in tumor cells via macrophage-mediated cytotoxicity in vitro [32,33]. Jenkins et al. demonstrated that a subclone of the human colon carcinoma cell line, DLD-1, which overexpresses iNOS, grows more slowly than parental DLD-1 cells in vitro [34]. Transfection of iNOS into murine melanoma cells has been shown to decrease their malignant potential [35], and $iNOS^{-/-}$ mice show increased ovarian sarcoma cell xenograft growth and metastasis as compared with wild-type $iNOS^{+/+}$ mice [36]. iNOS might be expressed in normal epithelial cells, while its expression may be reduced or undetectable in adenomas or carcinomas [37–40]. Recently, Scott et al. [41] reported that the targeted deletion of iNOS resulted in an increased number of small intestinal tumors in the $Apc^{Min/+}$ mouse. According to their report [41], adenoma development in $Apc^{Min/+}$ mice was associated with reduced expression of iNOS in the epithelial cells, suggesting that iNOS may have a protective, antineoplastic role, at least in the early stages of intestinal tumorigenesis. These previous investigations support the notion that iNOS-derived NO may be involved in the inhibition of tumor growth via mediating accelerated apoptosis.

Although gastric mucosal leukocyte accumulation in response to *H. pylori* was significantly increased in $iNOS^{-/-}$mice, the degree of gastric mucosal cell apoptosis was significantly attenuated without any significant change in the level of cellular proliferation in the gastric mucosa. These results suggest that iNOS or its derivatives may play a role in the induction of gastric

epithelial cell apoptosis and in the maintenance of normal cell turnover in *H. pylori*-infected inflamed gastric mucosa. The results obtained with *H. pylori*-colonized iNOS$^{-/-}$ mice might begin to fill the void in explaining the difference between wild-type mice and Mongolian gerbils; enhanced apoptosis in mice, as well as gastric mucosal proliferative changes and hyperplastic alterations, especially those observed in the long-term *H. pylori*-colonized gerbils, are not observed in iNOS$^{-/-}$ mice. Further investigation should be conducted to elucidate the tumorigenicity of *H. pylori*, and the role of long-term iNOS suppression and additional genetic modifications in this process.

Acknowledgements — This study was supported by a Grant-in-Aid for Scientific Research C (2) from Japan Society for the Promotion of Science (JSPS) (13670555, to H.S.), a Keio University Medical School Faculty and Alumni Grant (94-0009, to H.S.), and a grant from Ooyama Health Science Funds (to H.S.).

REFERENCES

[1] Uemura, N.; Okamoto, S.; Yamamoto, S.; Matsumura, N.; Yamaguchi, S.; Yamakido, M.; Taniyama, K.; Sasaki, N.; Schlemper, R. J. Helicobacter pylori infection and the development of gastric cancer. *N. Engl. J. Med.* **345:**784–789; 2001.

[2] Watanabe, T.; Tada, M.; Nagai, H.; Sasaki, S.; Nakao, M. *Helicobacter pylori* infection induces gastric cancer in Mongolian gerbils. *Gastroenterology* **115:**642–648; 1998.

[3] Honda, S.; Fujioka, T.; Tokieda, M.; Satoh, R.; Nishizono, A.; Nasu, M. Development of *Helicobacter pylori*-induced gastric carcinoma in Mongolian gerbils. *Cancer Res.* **58:**4255–4259; 1998.

[4] Suzuki, H.; Miyazawa, M.; Nagahashi, S.; Seto, K.; Kai, A.; Suzuki, M.; Miura, S.; Ishii, H. Attenuated apoptosis in *H. pylori*-colonized gastric mucosa of Mongolian gerbils in comparison with mice. *Dig. Dis. Sci.* **47:**90–99; 2002.

[5] Sakaguchi, A. A.; Miura, S.; Takeuchi, T.; Hokari, R.; Mizumori, M.; Yoshida, H.; Higuchi, H.; Mori, M.; Kimura, H.; Suzuki, H.; Ishii, H. Increased expression of inducible nitric oxide synthase and peroxynitrite in Helicobacter pylori gastric ulcer. *Free Radic. Biol. Med.* **27:**781–789; 1999.

[6] Li, C. Q.; Pignatelli, B.; Ohshima, H. Increased oxidative and nitrative stress in human stomach associated with cagA+ Helicobacter pylori infection and inflammation. *Dig. Dis. Sci.* **46:** 836–844; 2001.

[7] Watanabe, S.; Takagi, A.; Koga, Y.; Kamiya, S.; Miwa, T. Helicobacter pylori induces apoptosis in gastric epithelial cells through inducible nitric oxide. *J. Gastroenterol. Hepatol.* **15:** 168–174; 2000.

[8] Suzuki, H.; Mori, M.; Seto, K.; Kai, A.; Kawaguchi, C.; Suzuki, M.; Suematsu, M.; Yoneta, T.; Miura, S.; Ishii, H. *H. pylori*-associated gastric pro- and anti-oxidant formation in Mongolian gerbils. *Free Radic. Biol. Med.* **26:**679–684; 1999.

[9] Takahashi, S.; Keto, Y.; Fujita, H.; Muramatsu, H.; Nishino, T.; Okabe, S. Pathological changes in the formation of *Helicobacter pylori*-induced gastric lesions in Mongolian gerbils. *Dig. Dis. Sci.* **43:**754–765; 1998.

[10] Yamada, R.; Sartor, R. B.; Marshal, S.; Specian, R. D.; Grisham, M. B. Mucosal injury and inflammation in a model of chronic granulomatous colitis in rats. *Gastroenterology* **104:**756–771; 1993.

[11] Lowry, O. H.; Rosebrough, N. J.; Farr, A. L.; Randall, R. J. Protein measurement with the Folin phenol reagent. *J. Biol. Chem.* **193:**265–275; 1951.

[12] Smith, P. K.; Krohn, R. I.; Hermanson, G. T.; Mallia, A. K.; Gartner, F. H.; Provenzano, M. D.; Fujimoto, E. K.; Goeke, N. M.; Olson, B. J.; Klenk, D. C. Measurement of protein using bicinchoninic acid. *Anal. Biochem.* **150:**76–85; 1985.

[13] Grisham, M. B.; Hernandez, L. A.; Granger, D. N. Xanthine oxidase and neutrophil infiltration in intestinal ischemia. *Am. J. Physiol.* **252:**G567–G574; 1986.

[14] Dixon, M. F.; Genta, R. M.; Yardley, J. H.; Correa, P. Classification and grading of gastritis. The updated Sydney system. *Am. J. Surg. Pathol.* **20:**1161–1181; 1996.

[15] Misiewicz, J. J.; Tytgat, G. N. J.; Goodwin, C. S.; Price, A. B.; Sipponen, P.; Strickland, R. G. The Sydney Systems: a new classification of gastritis. Working Party Reports of the World Congress of Gastroenterology 1–12; 1990.

[16] Price, A. B. The Sydney system. Histological division. *J. Gastroenterol. Hepatol.* **6:**209–222; 1991.

[17] Gavrieli, Y.; Sherman, Y.; Ben-Sasson, S. A. Identification of programmed cell death in situ via specific labeling of nuclear DNA fragmentation. *J. Cell Biol.* **119:**493–501; 1992.

[18] Schlatt, S.; Weinbauer, G. F. Immunohistochemical localization of proliferating cell nuclear antigen as a tool to study cell proliferation in rodent and primate testes. *Int. J. Androl.* **17:**241–222; 1994.

[19] Brenes, F.; Ruiz, B.; Correa, P.; Hunter, F.; Rhamakrishnan, T.; Fontham, E.; Shi, T. Y. *Helicobacter pylori* causes hyperproliferation of the gastric epithelium: pre- and post-eradication indices of proliferating cell nuclear antigen. *Am. J. Gastroenterol.* **88:** 1870–1875; 1993.

[20] Mannick, E. E.; Bravo, L. E.; Zarama, G.; Realpe, J. L.; Zhang, X. J.; Ruiz, B.; Fontham, E. T.; Mera, R.; Miller, M. J.; Correa, P. Inducible nitric oxide synthase, nitrotyrosine, and apoptosis in Helicobacter pylori: effect of antibiotics and antioxidants. *Cancer Res.* **56:**3238–3243; 1996.

[21] Tatemichi, M.; Ogura, T.; Nagata, H.; Esumi, H. Enhanced expression of inducible nitric oxide synthase in chronic gastritis with intestinal metaplasia. *J. Clin. Gastroenterol.* **27:**240–245; 1998.

[22] Kim, J. M.; Kim, J. S.; Jung, H. C.; Song, I. S.; Kim, C. Y. Up-regulation of inducible nitric oxide synthase and nitric oxide in Helicobacter pylori-infected human gastric epithelial cells: possible role of interferon-gamma in polarized nitric oxide secretion. *Helicobacter* **7:**116–128; 2002.

[23] Kodama, K.; Sumii, K.; Kawano, M.; Kido, T.; Nojima, K.; Sumii, M.; Haruma, K.; Yoshihara, M.; Chayama, K. *Helicobacter pylori* infection increases serum nitrate and nitrite more prominently than serum pepsinogens. *Helicobacter* **7:**9–13; 2002.

[24] Kung, C. F.; Luscher, T. F. Different mechanisms of endothelial dysfunction with aging and hypertension in rat aorta. *Hypertension* **25:**194–200; 1995.

[25] Luscher, T. F.; Bock, H. A. The endothelial L-arginine/nitric oxide pathway and the renal circulation. *Klin. Wochenschr.* **69:** 603–609; 1991.

[26] Reckelhoff, J. F.; Kellum, J. A.; Blanchard, E. J.; Bacon, E. E.; Wesley, A. J.; Kruckeberg, W. C. Changes in nitric oxide precursor, L-arginine, and metabolites, nitrate and nitrite, with aging. *Life Sci.* **55:**1895–1902; 1994.

[27] Peek, R. M. J.; Hans-Peter, W.; Moss, S. F.; Yang, M.; Abdalla, A. M.; Tham, K. T.; Zhang, T.; Tang, L. H.; Modlin, I. M.; Blaser, M. J. *Helicobacter pylori* alters gastric epithelial cell cycle events and gastrin secretion in Mongolian gerbils. *Gastroenterology* **118:**48–59; 2000.

[28] Fox, J. G.; Li, X.; Cahill, R. J.; Andrutis, K.; Rustgi, A. K.; Odze, R.; Wang, T. C. Hypertrophic gastropathy in *Helicobacter felis*-infected wild type C57BL/6 mice and p53 hemizygous transgenic mice. *Gastroenterology* **110:**155–166; 1996.

[29] Suzuki, H.; Miyazawa, M.; Kai, A.; Suzuki, M.; Suematsu, M.; Miura, S.; Ishii, H. No Difference in the level of gastric mucosal cell apoptosis and proliferation in *H. pylori*-colonized *p53* heterozygous knockout mice. *Aliment. Pharmacol. Ther.* **16:**(Suppl. 2):158–166; 2002.

[30] Yamamoto, M.; Tsukamoto, T.; Sakai, H.; Shirai, N.; Ohgaki, H.; Furihata, C.; Donehower, L. A.; Yoshida, K.; Tatematsu, M. p53

knockout mice (−/−) are more susceptible than (+/−) or (+/+) mice to N-methyl-N-nitrosourea stomach carcinogenesis. *Carcinogenesis* **21:**1891–1897; 2000.

[31] Kiss, J.; Lamarque, D.; Moran, A. P.; Pozsar, J.; Morschl, E.; Laszlo, F.; Whittle, B. J. Helicobacter pylori lipopolysaccharide-provoked injury to rat gastroduodenal microvasculature involves inducible nitric oxide synthase. *Eur. J. Pharmacol.* **420:**175–179; 2001.

[32] Siedlar, M.; Mytar, B.; Krzeszowiak, A.; Baran, J.; Hyszko, M.; Ruggiero, I.; Wieckiewicz, J.; Stachura, J.; Zembala, M. Demonstration of iNOS-mRNA and iNOS in human monocytes stimulated with cancer cells *in vitro*. *J. Leukoc. Biol.* **65:**597–604; 1999.

[33] Cui, S.; Reichner, J. S.; Mateo, R. B.; Albina, J. E. Activated murine macrophages induce apoptosis in tumor cells through nitric oxide-dependent or -independent mechanisms. *Cancer Res.* **54:**2462–2467; 1994.

[34] Jenkins, D. C.; Charles, I. G.; Thomsen, L. L.; Moss, D. W.; Holmes, L. S.; Baylis, S. A.; Rhodes, P.; Westmore, K.; Emson, P. C.; Moncada, S. Roles of nitric oxide in tumor growth. *Proc. Natl. Acad. Sci. USA* **92:**4392–4396; 1995.

[35] Xie, K.; Huang, S.; Dong, Z.; Juang, S.-H.; Gutman, M.; Xie, Q.-W.; Nathan, C.; Fidler, I. J. Transfection with the inducible nitric oxide synthase gene suppresses tumorigenicity and abrogates gene metastasis in K-1735 murine melanoma cells. *J. Exp. Med.* **181:**1333–1343; 1995.

[36] Shi, Q.; Xiong, Q.; Wang, B.; Le, X.; Khan, N. A.; Xie, K. Influence of nitric oxide synthase II gene disruption on tumor growth and metastasis. *Cancer Res.* **60:**2579–2583; 2000.

[37] Moochhala, S.; Chhatwal, V. J.; Chan, S. T.; Ngoi, S. S.; Chia, Y. W.; Rauff, A. Nitric oxide synthase activity and expression in human colorectal cancer. *Carcinogenesis* **17:**1171–1174; 1996.

[38] Chhatwal, V. J.; Ngoi, S. S.; Chan, S. T.; Chia, Y. W.; Moochhala, S. M. Aberrant expression of nitric oxide synthase in human polyps, neoplastic colonic mucosa and surrounding peritumoral normal mucosa. *Carcinogenesis* **15:**2081–2085; 1994.

[39] Ropponen, K. M.; Kellokoski, J. K.; Lipponen, P. K.; Eskelinen, M. J.; Alanne, L.; Alhava, E. M.; Kosma, V. M. Expression of inducible nitric oxide synthase in colorectal cancer and its association with prognosis. *Scand. J. Gastroenterol.* **11:**1204–1211; 2000.

[40] Hao, X. P.; Pretlow, T. G.; Rao, J. S.; Pretlow, T. P. Inducible nitric oxide synthase (iNOS) is expressed similarly in multiple aberrant crypt foci and colorectal tumors from the same patients. *Cancer Res.* **61:**419–422; 2001.

[41] Scott, D. J.; Hull, M. A.; Cartwright, E. J.; Lam, W. K.; Tisbury, A.; Poulsom, R.; Markham, A. F.; Bonifer, C.; Coletta, P. L. Lack of inducible nitric oxide synthase promotes intestinal tumorigenesis in the $Apc^{Min/+}$ mouse. *Gastroenterology* **121:**889–899; 2001.

Bilirubin Rinse: A Simple Protectant Against the Rat Liver Graft Injury Mimicking Heme Oxygenase–1 Preconditioning

Yutaro Kato,[1,2] Motohide Shimazu,[2] Mieko Kondo,[1] Koji Uchida,[3] Yusuke Kumamoto,[2] Go Wakabayashi,[2] Masaki Kitajima,[2] and Makoto Suematsu[1]

Heme oxygenase (HO)-1 preconditioning through genetic or pharmacologic interventions was shown experimentally to improve posttransplant outcome of liver grafts. However, its clinical application requires careful consideration because of the complexity and economic costs of the procedures. This study aimed to examine if graft preconditioning with HO-1 could be substituted by a simple treatment with heme-degrading products such as bilirubin. Rats were pretreated with or without hemin, an HO-1 inducer for preconditioning. Their livers were harvested as grafts in University of Wisconsin (UW) solution for 16 hours at 4°C and followed by reperfusion *ex vivo* or by transplantation *in vivo*. The control grafts were also treated with a rinse buffer containing varied concentrations of unconjugated bilirubin with different time intervals. The HO-1–preconditioned grafts *ex vivo* exhibited a marked improvement of bile output and cell injury that was cancelled by blocking HO with zinc protoporphyrin-IX. The aggravation of the graft viability by the inhibitor was repressed by supplementation of bilirubin but not by that of carbon monoxide. Furthermore, a short-term rinse treatment with micromolar levels of bilirubin attenuated biliary dysfunction and cell injury of the grafts both *ex vivo* and *in vivo* even without HO-1 preconditioning. The protective effects of HO-1 preconditioning or bilirubin rinse appeared to involve its inhibitory effects on lipid peroxidation in hepatocytes. In conclusion, these results suggest that bilirubin rinse serves as a simple strategy to ameliorate hyperacute oxidative stress and hepatobiliary dysfunction of the transplanted grafts, mimicking effects of HO-1–mediated preconditioning. (HEPATOLOGY 2003;38:364-373.)

See Editorial on Page 286

In liver transplantation, control of acute hepatobiliary dysfunction elicited by cold ischemia-reperfusion (CI/R) remains to be achieved to further improve posttransplant outcome.[1,2] Such a dysfunction involves primary graft nonfunction that is characterized by severely impaired bile formation initiating from the hyperacute phase of reperfusion.[3] Proinflammatory mediators generated on CI/R such as oxygen free radicals and inflammatory cytokines give rise to insults to nonparenchymal cells[1,2,4,5] and to hepatocytes.[6] Recent studies suggest that the donor grafts undergoing pre–cold ischemic conditioning become resistant to reperfusion injury. Several different protocols have been shown to account for such preconditioning procedures: Kupffer cell inactivation or depletion,[7,8] induction of heat shock proteins,[9,10] and short-term ischemia before cold storage.[11]

Besides these protocols, overexpression of heme oxygenase 1 (HO-1) by gene transfection or by the enzyme inducers has been shown experimentally to benefit posttransplant liver and heart graft viability.[12,13] Pretreatment of genetically obese Zucker rats with pharmacologic inducers of HO-1 improved post-CI/R viability of the liver graft,[12] suggesting that the preconditioning could expand the supply of usable donor livers. HO-1 is the inducible HO isozyme that degrades protoheme IX into free diva-

Abbreviations: CI/R, cold ischemia/reperfusion; HO, heme oxygenase; UW, University of Wisconsin; LDH, lactate dehydrogenase; ZnPP, zinc protoporphyrin-IX; CuPP, copper protoporphyrin-IX.

From the Departments of [1]Biochemistry and Integrative Medical Biology and [2]Surgery, School of Medicine, Keio University, Tokyo, Japan; and [3]Department of Food and Biodynamics, Graduate School of Bioagricultural Sciences, Nagoya University, Nagoya, Japan.

Received February 8, 2003; accepted May 1, 2003.

Supported by a grant-in-aid for Creative Scientific Research by the Japan Society for the Promotion of Science 16GS0015 and by the 21st Century Center-of-Excellence Program and the Leading Project for Biosimulation from the Ministry of Education, Sciences and Technology in Japan and partly by a grant from Keio University School of Medicine.

Address reprint requests to: Makoto Suematsu, M.D., Ph.D., Department of Biochemistry and Integrative Medical Biology, School of Medicine, Keio University, 35 Shinanomachi, Shinjuku-ku, Tokyo 160-8582, Japan. E-mail: msuem@sc.itc.keio.ac.jp; fax: (81) 3-3358-8138.

0270-9139/03/3802-0013$30.00/0

doi:10.1053/jhep.2003.50300

lent iron, carbon monoxide (CO), and biliverdin-IXα, a substrate for biliverdin reductase to generate bilirubin-IXα.[14] Although these HO-derived products are all biologically active,[15-18] which products play a major role in the protection mechanism remains unknown. Uncovering such a mechanism could allow us to find a novel and simple method to ameliorate posttransplant graft injury.

This study aimed to show such mechanisms underlying the beneficial effects of HO-1 preconditioning against CI/R-induced liver dysfunction *in vivo*. The current results show that bilirubin rather than CO accounts for a crucial factor that ameliorates CI/R-induced hepatobiliary dysfunction. Furthermore, a simple supplementation of this bile pigment for the pretransplant graft rinse significantly attenuated CI/R-induced dysfunction without any preconditioning interventions for the enzyme induction. The current results not only clarified involvement of bilirubin in protection mechanisms but also shed light on the usefulness of the bilirubin rinse as a potentially therapeutic stratagem against posttransplant reperfusion injury.

Materials and Methods

Preparation of Liver Grafts and the HO-1 Preconditioning. All experimental protocols for care and use of animals in the current study were approved by the institutional guidelines of Keio University School of Medicine. Male Wistar rats weighing 190 to 230 g were allowed free access to laboratory chow and water. The rats were fasted for 6 hours and then treated with an intraperitoneal injection of hemin (40 μmol/kg), a potent inducer of HO-1, or saline as vehicle. Subsequently, animals were fasted for 18 hours before graft harvest. As described elsewhere,[19] the present protocol of hemin treatment caused an induction of HO-1 protein at a maximum level concurrently with a marked increase in the venous CO flux and biliary excretion of bilirubin-IXα. Based on these data, this time interval was chosen as an optimal protocol to investigate effects of HO-1 on post–cold ischemic graft dysfunction.

These rats were anesthetized with an intraperitoneal injection of pentobarbital sodium (40 mg/kg body wt). The common bile duct was cannulated for collection of bile samples.[19,20] The portal vein was cannulated with a 16-gauge catheter and flushed with 20 mL lactated Ringer's solution kept at 4°C. The liver was perfused subsequently with 20 mL University of Wisconsin (UW) solution at the same temperature and harvested in the same solution for 16 hours at 4°C. We chose 16 hours for the storage duration because this protocol for cold ischemia exhibited acute oxidative stress on reperfusion as judged by hydroperoxide generation with a reduction of bile formation.[6] After completing the storage, the liver graft was reperfused through the portal vein at a constant flow of 4 mL/min/g liver with the Krebs-Henseleit buffer saturated with carbogen (pH 7.4, 37°C) for 40 minutes in the presence of sodium taurocholate at 30 μmol/L.[6]

Determinations. Western blot analysis was performed in several groups of the liver grafts to determine HO-1 protein expression.[21] When necessary, the flux of CO in the hepatic venous effluent was measured according to our previous methods.[17] Bile samples were collected every 5 minutes during the 40-minute reperfusion period. Concentrations of bilirubin-IXα in bile samples were determined by an enzyme-linked immunosorbent assay.[22,23] Concentrations of total bile salts and phospholipids were determined by an enzyme inhibition assay.[24] To determine hepatocellular damages, contents of lactate dehydrogenase (LDH) and aspartate aminotransferase released into the hepatic venous perfusate were measured with standard assay techniques.

Interventions. To examine the roles of HO activity in regulation of reperfusion-induced graft dysfunction, zinc protoporphyrin-IX (ZnPP; Porphyrin Product, Milwaukee, WI), a potent HO inhibitor, or copper protoporphyrin-IX (CuPP; Porphyrin Product), a metalloprotoporphyrin that does not inhibit its enzymatic activity, was applied to the buffer solution at 1 μmol/L on reperfusion of the hemin-pretreated liver grafts. Separately, either bilirubin (Sigma Chemical Co., St. Louis, MO) or CO at varied concentrations was coperfused in the presence of 1 μmol/L ZnPP on reperfusion of the HO-1–preconditioned liver grafts. When necessary, both bilirubin and CO were perfused simultaneously. Separately, effects of supplementation of bilirubin were examined at varied doses after reperfusion in the grafts without hemin pretreatment.

Determination of an Oxidative Stress–Derived Product in the Liver Grafts. Immunohistochemical analysis was performed using a monoclonal antibody 5F6, which recognizes protein-bound acrolein, an end product generated through lipid peroxidation on oxidative stress.[25] The 16-hour cold ischemic liver grafts undergoing different treatment procedures followed by 30-minute reperfusion were subjected to this examination. As shown in Results, nuclei of hepatocytes constituted a main intracellular compartment indicating positive immunoreactivities of 5F6 in the grafts. The number of hepatocytes with 5F6-positive nuclei per a unit area (0.04 mm^2) was counted in 10 randomly selected high-power fields (×400).

In Vivo *Transplantation Model.* For orthotopic syngeneic transplantation of the liver, inbred male Lewis rats weighing 220 to 280 g were free of access to water and

fasted for 24 hours before transplantation and were used for the donors and recipients. In the HO-1 preconditioning group, rats were treated with hemin 18 hours before graft procurement. Liver transplantation was performed according to techniques by Kamada and Calne with some modification.[26] Briefly, in the donors, abdominal organs including the liver were flushed through the abdominal aorta with 20 mL lactated Ringer's solution at 4°C. A total of 20 mL cold UW solution was then infused slowly into the liver through the aorta and the portal vein. The common bile duct was cannulated with a PE-10 catheter for collection of bile samples. The liver with the common bile duct cannulation was procured as the graft and preserved in UW solution for 16 hours at 4°C.

In the recipient operation, the liver graft was implanted orthotopically without arterial reconstruction.[26] At the end of the storage period, the liver grafts underwent pretransplant rinse via the portal vein with 7 mL lactated Ringer's solution at 4°C. When necessary, bilirubin at varied concentrations was added to the rinse solution. The recipients surviving for 24 hours were killed under ether anesthesia.

Indices for Efficacy and Accessibility of Bilirubin for Graft Protection. After the implantation procedure was completed, bile output was monitored at 30 minutes and 24 hours after the onset of portal reperfusion. Serum levels of aspartate aminotransferase, alanine aminotransferase, and LDH at 24 hours were determined. Posttransplant 24-hour survival was compared among groups. We also performed immunohistochemical detection of bilirubin in the grafts using the anti–bilirubin-IXα monoclonal antibody 24G7.[27]

Statistics. Statistical analyses among some groups were performed using one-way ANOVA and Fisher's multiple comparison tests. Posttransplant 24-hour survival was analyzed by χ^2 test. Results were expressed as mean ± SE, and $P < .05$ was considered significant.

Results

Alterations in Expression of HO-1 and CO Generation in the Hemin-Pretreated Liver Grafts. Figure 1 shows hemin-induced alterations in expression of HO-1 and CO generation in the 16-hour cold ischemic liver grafts. As seen in Fig. 1A, the 16-hour cold storage (C16) did not cause any notable induction of HO-1 in the grafts. When pretreated with hemin (hemin [+]), grafts exhibited marked elevation of HO-1 expression concurrently with an elevation of CO in the venous perfusate (Fig. 1B). The grafts increased their expression of HO-1 slightly in the C16 (lane d) or C16 plus 30-minute reperfusion group (lane e, C16 + R). Under these circumstances, the venous CO flux was approximately 3-fold greater than that in the hemin-untreated group (C16 in the hemin [−] group) although smaller than the value measured in the non–cold ischemic control in the hemin-treated group (control in the hemin [+] group). These results suggest that the hemin-treated liver grafts increase their ability to generate CO through an induction of HO-1.

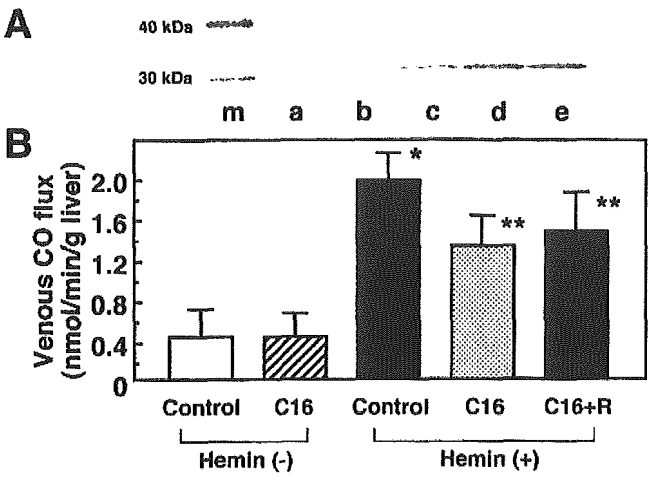

Fig. 1. Alterations in expression of HO-1 protein and generation of CO in perfused rat livers undergoing 16-hour cold storage and reperfusion. (A) Western blot analysis of the HO-1 protein expression (32 kd) using the anti-rat HO-1 monoclonal antibody GTS-1. **Lane m,** molecular markers (30 and 40 kd). **Lanes a and b** indicate the data from livers treated without and with 16-hour cold storage (C16), respectively. **Lanes c, d, and e** are from hemin-pretreated livers with different treatment procedures; c, a graft pretreated with hemin; d, a hemin-pretreated graft undergoing 16-hour cold storage alone; e, a hemin-pretreated graft undergoing cold storage followed by 30-minute reperfusion (R). (B) Differences in the venous flux of CO among those groups. Note that the venous CO flux in the 16-hour cold storage livers (C16) is comparable to that in intact livers (control). Hemin (+) and Hemin (−), pretreatment with and without hemin at 18 hours before the start of cold storage, respectively. Data represent mean ± SE of 4 separate experiments. *$P < .05$ and **$P < .05$ compared with the hemin-untreated control livers and those undergoing 16-hour cold storage, respectively.

Improved Recovery of Bile Output in the HO-1 Preconditioning Liver Grafts. Figure 2 shows differences in the recovery of bile output after reperfusion among groups. Bile output in the hemin-untreated C16 grafts increased time dependently and reached a plateau level that was significantly lower than the hemin-untreated control grafts. This result supported a notion that C16 treatment causes hepatobiliary dysfunction, which is in good agreement with that in our previous study.[6] When the grafts were pretreated with hemin (hemin/C16), the bile output displayed a rapid recovery at 10 minutes and became greater than that in the C16 group. Such an improving effect of the HO-1 preconditioning was markedly suppressed by coperfusion of ZnPP, an HO inhibitor. The ZnPP-induced difference in the decrease